Hindawi

Research Article

Magneto-Rotational Augmentation of Bioconvective Transport in Plasma-Nanofluid Flowing through a Penetrable Spinning Disc

Ebenezer Olubunmi Ige [1,2] **Isaac Folorunso Odesola,**[2] **Sikiru Babatunde Ayedun,**[2] **and Olusegun M. Ilori**[3]

[1]*Department of Mechanical and Mechatronic Engineering, Afe Babalola University, Ado Ekiti, Nigeria*
[2]*Faculty of Technology, Department of Mechanical Engineering, University of Ibadan, Ibadan, Nigeria*
[3]*School of Engineering and the Built Environment, Birmingham City University, Birmingham, UK*

Correspondence should be addressed to Ebenezer Olubunmi Ige; ige.olubunmi@abuad.edu.ng

The phenomenon of bioconvective transport through the manipulation of motile microorganisms is considered a promising process control technique in several biological processes and microdevices. Inducing convective transport in self-propelling microbes could be tailored to improve mixing, reaction propensity, and concentration transport within the media. This paper examined the combined effect of magnetic and rotational fields on the argumentation of bioconvective transport in the nanofluid-mediated plasma flow. A detailed analysis of the transport and dynamics of reactive forces during bioconvection in a rotary disc-like microchannel is presented. The physics of the problem was described by coupled nonlinear ordinary differential equations, which were numerically computed using the spectral relaxation scheme of the spectral homotopy analysis method. It was observed that the imposition of a magnetic field constituted viscous drag in the plasma-nanofluid media, which consequently increases the thermophoretic parameter in the bioconvective flow. It was ascertained that coupled magnetic and rotational effects significantly augmented the motility of microorganisms and translated to growth in momentum and concentration fields which is noticeable in the generation of stretching effect on the bacterium-containing plasma-nanofluid flow. The findings of this study could provide an essential basis for the design of bioreactors, centrifugal microfluidics technologies, and microdevices for use in a broad spectrum of biotechnology.

1. Introduction

Bioconvection is the unique streamlines of flow fields generated by self-propelling microorganisms that can be utilized as a tool in creating serial microscale technologies in biotechnology and other domains of life sciences. This may be achieved via the miniaturization of fluidic devices which is currently being demonstrated on a microfluidic platform. The credentials of microfluidics have been proven which include its potential to administer precise control and handle manipulations in fluidic media for target purposes [1, 2]. Moreover, several outstanding contributions employing principles of microfluidics proved to be beneficial across a spectrum of biomedical science and biotechnology.

Importantly, the ease of microfabrication and geometric control of fluidic conduits in addition to the precise regulation of living cells in microfluidic devices have positioned microfluidic devices as a promising platform for microbial and ecological investigations [3–6]. Within miniaturized fluidic conduits, reengineering of the microenvironment can be achieved to capture microbial motility and cell-level activities such as cell-level differentiation of genotypic and phenotypic variations in the bacterial population [7–12] Intricate movements that depict microbial activities such as bioconvection could be investigated to provide detailed visualization required to study the dynamics of gyrostatic in microbe-laden fluids in micron-sized conduits [13–15]. Although the cost of microfabrication is competitive,

experimentation in micrometer scale requires expensive and elaborate imaging technology for flow visualization [15, 16]. Therefore, a numerical investigation is been sought as a precursor to experimentation and to provide rigorous analysis of bioconvective transport in motile microbial cells inhabiting a microengineered conduit.

In the family of nanotechnology, carbon nanotubes (CNTs) have been considered to be a creditable candidate in thermal management. The study in [17] presented mathematical investigation on single-walled carbon nanotubes (SWCNTs) for utilization thermal management. The study in [18] reported bioconvection in a stratified motile microorganism in fluid media to investigate the role of activation energy on the dynamics using the popular numerical shooting scheme. A similar study in [19] showed magnetic field-induced transport in a bioconvection scenario over a wedged surface in a Carreau-type non-Newtonian fluid domain. The study in [20] investigated thermal flux and reaction regime in a modelled Eyring–Powell rheology class of non-Newtonian fluid. The study in [21] showed the potential of scaling lie-group analysis to handle bioconvection for micropolar fluids through a fibrous medium. The study in [22] proposed a self-similar convection strategy to study concentration transport in a rotatory cone-like perforated. The study in [23] showed that a combination of thermal and reaction optimization can be achieved by suction in the premise of Karman swirling flow. Over a rotating disc-like member, the work in [24] studied simultaneous biograde and nanograde convection in a Stefan-type fluid. The authors numerically showed that thermal transfer is achieved via suction. A similar investigation by the same group examined the incidence of Navier slip under the influence of magnetic field in the premise of a flat substrate [25]. Amirsom et al. presented a three-dimensional approach to understanding anisotropic slip formation in bioconvection flow over stretching plates [26].

The magnetic field is projected as a promising candidate to actualize controlled formation of bioconvective flows in bacterial cells for which ongoing progress in numerical methods have captured magneto-taxis (magnetotactic) for propulsion of bacterial cells in fluid media [27]. The Buongiorno model was demonstrated to analyze magnetic field-mediated convection in nanofluid containing gyrotactic microorganisms [28]. The report of Chakraborty et al. revealed that using a traditional boundary value scheme the propulsion rate of motile microorganisms could be controlled by the behaviour of convective transport at the surface [29]. The dominating influence of thermophysical parameters such as the duo of Lewis and Peclet numbers constitutes an increase in density of self-propelling microorganisms in the presence of magnetic field [30]. The study of Mutuku and associates presented numerical treatment of magnetohydrodynamic flow in nanofluid containing unstable microorganisms leveraging on the Runge–Kutta-Fehlberg scheme. The authors showed in semblance to the work of Pal and Mondal [30] that a combinatory effect of the earlier bioconvective parameter influences the propagation

of migrating microorganisms [31]. Thermal energy generated by an imposed magnetic field effect is considered to impact the flow regime in bioconvection-driven fluids. This analysis was reported using the augmented continuum expression over Boussinesq approximation to show that overall streamline patterns generated by magnetic field-influenced bioconvective transport facilitated rapid thermal distribution and oxygen convection [32]. Shehzad and his team showed that magnetic field imposition around the domains of motile microbes could be tailored to moderate angular rotation of the motile microorganism [33].

It is established that bacterial and all motile microorganisms possess inherent sensitivity and their response to rotational impulses could stimulate activities like swirling and swimming in the fluid media. Rotation-induced bioconvection was captured in the numerical analysis of two rotating plates immersed in nanofluid [34]. Waqas and co-workers numerically described the behaviour of Oldroyd-B nanofluid containing highly mobile microorganisms [35]. Considering the rheology of nanofluid to follow the Jeffrey model, a group of researchers employed the technique of homotopy analysis to describe the bioconvection in a conic vessel under the dual effect of magnetic field and rotation [36]. Analysis of biothermal reactions was conducted using the homotopy method to describe the important physics of bioconvection in Buongiorno nanofluid [37]. A few reports have considered the combined effect of magnetic field and mechanical-induced rotation on the subject of bioconvection. Earlier studies showed that continuous disc rotation depends on the supply of substantial rotational torque which translates to significant velocity spreading within the media and consequently the experience of declined thermal transport [38]. Tuz-Zohra et al. numerically examined by generating similarity transformation for the problem where a biocompatible nanoparticle coated with microorganisms is exposed to the combinatory effect of magnetic field and mechanical rotational forces. The authors revealed that the magnetic field at escalating magnitudes contributes to the uphill glide motility profile in embedded microorganisms [24]. Over a stretching rotating disc, suction-assisted heat transfer intensification was achieved by numerically computing via the Runge–Kutta–Fehlberg method [39]. Three-dimensional analysis of bioconvection in nanofluid flowing through a rotating disc with the treatment of nanofluid as a power-law model illustrates the density of self-propelling microorganism depends on the coupled effect of radiation parameter and the coefficient of Brownian motion [40].

Over the last two decades, emerging solutions around medical diagnostics have leveraged innovations in the corridor of nanotechnology on which the study of nanofluidics is premised. Nanoparticles have been utilized in a number of avenues to address challenges in cancer detection [41], intervention in the coronavirus pandemic [42], creatine identification [43], desalination [44]; vaccine delivery in blood lymph node [45], nanotherapy in abdominal aneurysm [46, 47], and detection and management of leukemia

[48]. In principle, the dispersion of nanoparticles in fluid media for the transport of target species is treated as nanofluid. There are a number of routes by which nanoparticles can gain admittance into the human body, namely, food intake and intravenous and intracutaneous injections [49]. This in-body dispersion of nanoparticle creates interaction with biomolecules, and this environment stimulates the formation of a corona of molecule and biomolecule-nanoparticle complex with plasma serving as the base fluid. The inclusion of nanoparticles in the bloodstream and other body fluids is crusaded as the characteristic features of near-generation medical devices; thereby the increase in its application in many point-of-care devices [50]. Particularly in biomicrofluidics, metallic, nonmetallic, and polymer-based nanoparticles are being considered in the design of diagnostics tools on microfluidics platforms.

Within the purview of nanofluidics, Brownian and thermophoretic parameters are considered to possess controlling effects in the analyses of bioconvection in microorganism-mediated flow confinement. Amirsom and coworkers [26] showed that the increasing the Brownian parameter corresponds to a stronger thermophoretic force within the fluid domain which encourage the transport of nanoparticle. This invariably translates to increasing nanoparticle volume fraction in the neighbourhood of the boundary layer. Beg and coworkers implemented the Lie-group scheme on magnetoconvective flow in an electrically-mediated flow environment. This group of researchers illustrated that no slip was acheived by increasing Nusselt number while uprise in the Richson parameter resulted in thickening of the thermal boundary layer under decimated Biot number of 0.1 scenario [51]. Invariably, the hydrodynamic slip parameter swells under these conditions according to the observations reported in the literature. The company of Uddin employed a linear-group transformation technique to investigate the impact of radiative flux on idealized scenarios of multiple slip-on momentum, with thermal and concentration fields premised on a conjugated Runge–Kutta–Fehlberg fifth-order quadrature scheme [52]. Zhora and fellows numerically illustrated the dynamics of nonfluid under the influence of rotational force in the presence of microorganisms. The report showed that thermal transport and concentration flux are controlled by an override effect of suction [24]. The same group of authors showed that for biological grade nanoliquid, under elevated blowing condition, a significant boundary layer thickness is reported while their observation elucidates flow acceleration with high wall slip parameters [53].

Notable observation in the subject of nano-bioconvection on a porous substrate with thermal consideration for Boussinesq approximation has carried sufficient research interest. The study in [54] performed numerical experiment to show that momentum decline with escalating blowing function and conjugated quantities of Darcy, power-law index cum proscribed minute-size pore shape parameters. The study in [55] utilized the Boussinesq approximation and reported remarkable bioconvection and thermal transport

with decimated activation energy, thermal, and chemical parameters in a motile organism-based fluidic media flowing over a perforated substrate. The study in [56] employed the duo of Pedley and Kessler models to analyze the flow of gyrotactic organisms while evaluating the parameters such as Peclet, Rayleigh, and associated nondimensional quantities in microorganism-filled media. Balla et al. [57] illustrated using numerical scheme to investigate flow in microorganism-based flows under the Boussinesq assumption based on identified controlling parameters such as Rayleigh and chemical parameters. The studies revealed the superlative effect of swimming parameters in motile organism-mediated transport media. The study in [58] explored convective transport of nanoliquid flow mediated by motile microorganisms over a perforated substrate in the vicinity of magnetic field imposition. The study analyzed heat transfer over varied properties of nanoparticles and showed that thermal and momentum intensity was higher for certain nano-oxide while recording escalating magnitudes of Nusselt and Rayleigh parameters in the neighbourhood of magnetic field. The study of Balla and Naikoti [59] revealed that momentum transport is strengthened by the Rayleigh parameter and Peclet number while thermal transport is strongly connected to the magnetic field parameter under a scenario of iss concentration of oxygen in microorganism-based media. Jamuna and Balla [60] adopted Boussinesq approximation to examine the Darcy-type flow in a porous confinement using Gerkain-based finte element scheme and identified the duo of Peclet and Buyancy played a dominant role in determination of isocentration of nanooxied and motile orgamisms with special consideration.

In this work, emphasis is directed towards the contribution of magnetic field in augmenting the bioconvection of motile bacterium in a plasma stream which is considered a complex fluid. Important physics required to delineate the dynamics of locomotion of microorganisms in the media under the effect of externally imposed magnetic field is analyzed using the established SHAM technique. Magnetic field augmentation impacts the microbe capture and rotation of the thin circular disc, while the manifestation of transport phenomena within the fluid media is described and inference to purification in the plasma stream is methodically presented. This finding may openly focus on the paradigm of nanoparticle-mediated capture of motile microorganisms by controlling the incidence of bioconvection which could open a new paradigm in the broad area of microdevice technology for medical applications.

2. Description of the Problem

Substantial thrust in numerical computation has been devoted to the consideration of bioconvection in convectional fluid and nanofluid having water as its base fluid. Recent findings proved that tailored bioconvection can be considered a tool for purifying bacterial pollution in a broad spectrum of fluid media [61–63]. In this study, the problem
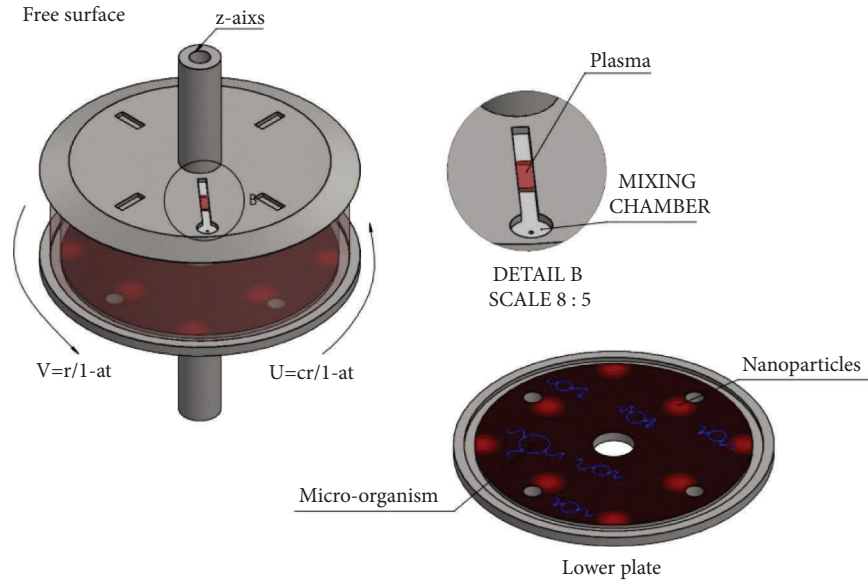
FIGURE 1: Schematic representation of microbe-containing circular disc microfluidics device mounted on a rotor.

of purifying bacterial-polluted fluid media is investigated by utilizing bioconvection as a tool to engulf microorganisms leveraging on techniques of numerical analysis. It considered bacterial-containing blood plasma (treated as Casson fluid) is contained in micromachined confinements of the thin circular discs while the activities of microorganisms in plasma suspension are predicted to trigger bioconvection in the circular disc plate (see Figure 1). The inclusion of magnetic nanoparticles is considered for engulfing a unique population of microorganisms. In the process, the low-density nanoparticle-bacterial conjugate gives raise to bioconvective transport with the fluid media. The magnetic field is imposed around the circular disc (CD) to augment bioconvective transport and nanoparticle-bacterium conjugation, thereby purifying the stream of plasma in the rotating disc.

2.1. Mathematical Analysis. Consider an unsteady laminar, incompressible, and bioconvective flow of magnetized Casson nanofluid with gyrotactic microorganisms. The flow is considered to be rotating and stretching in a penetrable disk. Close to the origin of a cylindrical coordinate system, a thin elastic disk is assumed to be radially narrow. The flow analysis is set up based on the following assumptions:

(i) The disk is assumed to be stretchable with variable viscosity and thermal conductivity.

(ii) The circular disk stretches with a velocity of $u = cr/(1 - at)$. It is also assumed to rotate with a uniform velocity $v = r\Omega/(1 - at)$ in the azimuthal direction.

(iii) A diffusing nanoparticle is assumed to be situated at the rotating disk.

(iv) At the surface of the disk, T_0, C_0, and N_0 are considered to be the temperature, concentration, and microorganism.

(v) The reference temperature, concentration, and microorganism are denoted by T_{ref}, C_{ref}, and N_{ref}, respectively.

(vi) The imposed magnetic field is assumed to be time-dependent with the magnitude towards the z-axis described as $B(t) = B_0/\sqrt{1 - at}$.

(vii) The concentration of nanofluid species in the plasma-microorganism complex is assumed to be high such that Soret and Dufour effects are taken to be significant.

(viii) We considered a remodification of the energy equation for nonlinear thermal radiation. Also, the species concentration is assumed to possess activation energy with the Arrhenius expressions.

Based on the above assumptions, the boundary layer equations in accordance with [64] become the following:

$$\frac{\partial u}{\partial r} + \frac{u}{r} + \frac{\partial w}{\partial z} = 0, \tag{1}$$

$$\frac{\partial u}{\partial t} + u\frac{\partial u}{\partial r} + w\frac{\partial u}{\partial z} - \frac{v^2}{r} + \lambda_1\left[\frac{\partial^2 u}{\partial t^2} + 2u\frac{\partial^2 u}{\partial r\partial t} - 2\frac{v}{r}\frac{\partial v}{\partial t} + 2w\frac{\partial^2 u}{\partial z\partial t} - \frac{2uv}{r}\frac{\partial v}{\partial r} + \frac{uv^2}{r^2} + 2uw\frac{\partial^2 u}{\partial r\partial z} - \frac{2vw}{r}\frac{\partial v}{\partial z} + \frac{v^2}{r}\frac{\partial u}{\partial r} + w^2\frac{\partial^2 u}{\partial z^2}\right]$$
$$= \frac{1}{\rho}\left(1 + \frac{1}{\beta}\right)\frac{\partial}{\partial z}\left(\mu(T)\frac{\partial u}{\partial z}\right) - \frac{\sigma_e B(t)^2}{\rho_f}\left(u + \lambda_1\left(\frac{\partial u}{\partial t} + w\frac{\partial u}{\partial z}\right)\right) \tag{2}$$
$$+ \frac{1}{\rho_f}\left[(1 - c_f)\rho_f\beta^* g^*(T - T_\infty) - (\rho_p - \rho_f)g^*(C - C_\infty) - (N - N_\infty)g\gamma^*(\rho_m - \rho_f)\right],$$

$$\%\frac{\partial v}{\partial t} + u\frac{\partial v}{\partial r} + w\frac{\partial v}{\partial z} + \frac{uv}{r}$$
$$+ \lambda_2\left[\frac{\partial^2 v}{\partial t^2} + 2u\frac{\partial^2 v}{\partial r\partial t} + \frac{2v}{r}\frac{\partial u}{\partial t} + 2w\frac{\partial^2 v}{\partial z\partial t} + u^2\frac{\partial^2 v}{\partial r^2} - \frac{2u^2 v}{r^2} + \frac{2uv}{r}\frac{\partial u}{\partial r} + 2uw\frac{\partial^2 v}{\partial r\partial z} - \frac{v^3}{r^2} + \frac{2vw}{r}\frac{\partial u}{\partial z} + w^2\frac{\partial^2 v}{\partial z^2} + \frac{v^2}{r}\frac{\partial v}{\partial t}\right]$$
$$= \frac{1}{\rho}\left(1 + \frac{1}{\beta}\right)\frac{\partial}{\partial z}\left(\mu(T)\frac{\partial v}{\partial z}\right) - \frac{\sigma_e B(t)^2}{\rho_f}\left[v + \lambda_2\left(\frac{\partial v}{\partial t} + w\frac{\partial v}{\partial z}\right)\right], \tag{3}$$

$$\frac{\partial T}{\partial t} + u\frac{\partial T}{\partial r} + w\frac{\partial T}{\partial z} = \frac{1}{\rho c_p}\frac{\partial}{\partial z}\left(k(T)\frac{\partial T}{\partial z}\right) - \frac{1}{\rho c_p}\frac{\partial q_r}{\partial z} + \tau\left[D_B\frac{\partial T}{\partial z}\frac{\partial C}{\partial z} + \frac{D_T}{T_0}\left(\frac{\partial T}{\partial z}\right)^2\right]$$
$$+ \frac{D_m k_T}{c_s c_p}\frac{\partial^2 C}{\partial z^2} + \frac{\sigma_e B(t)^2}{\rho}(u^2 + v^2) + \frac{\mu}{\rho c_p}\left(\frac{\partial u}{\partial z}\right)^2 + \frac{\sigma_e B(t)^2}{\rho c_p}u^2 + \frac{Q_0}{\rho c_p}(T - T_0), \tag{4}$$

$$\frac{\partial C}{\partial t} + u\frac{\partial C}{\partial r} + w\frac{\partial C}{\partial z} = D_B\frac{\partial^2 C}{\partial z^2} + \frac{D_T}{T_0}\frac{\partial^2 T}{\partial z^2} - K_l^2(C - C_0)\left(\frac{T}{T_0}\right)^2\exp\left(-\frac{E_a}{K_1 T}\right) + \frac{D_m k_T}{T_m}\frac{\partial^2 T}{\partial z^2}, \tag{5}$$

$$\frac{\partial N}{\partial t} + u\frac{\partial N}{\partial r} + w\frac{\partial N}{\partial z} + \frac{b^* W_c}{(C_w - C_0)}\left[\frac{\partial}{\partial z}\left(N\frac{\partial C}{\partial z}\right)\right] = D_m\frac{\partial^2 N}{\partial z^2}. \tag{6}$$

The following boundary conditions are applied in accordance with [64]:

$$u = \frac{cr}{1 - at},$$
$$v = \frac{c\Omega}{1 - at},$$
$$w = 0,$$
$$T = T_s, \tag{7}$$
$$C = C_s,$$
$$N = N_s,$$
$$\text{at } z = 0,$$

$$\frac{\partial u}{\partial z} = \frac{\partial v}{\partial z} = 0,$$
$$w = \frac{\partial h}{\partial t} + u\frac{\partial h}{\partial r}, \tag{8}$$
$$\frac{\partial T}{\partial z} = \frac{\partial C}{\partial z} = \frac{\partial N}{\partial z} = 0,$$
$$\text{at } z = h,$$

where T_s, C_s, N_s, $\mu(T)$, $k(T)$, and ν are the interfacial temperature, concentration of self-propelling microorganism, temperature-dependent dynamic viscosity, temperature-dependent thermal conductivity, and kinematic viscosity, respectively. Also, σ_e, β^*, g^*, B_0, ρ_f, $B(t)$, T_∞, D_T, and $\tau = (\rho c)_p/(\rho c)_v$ represent electrical conductivity, volume suspension coefficient, acceleration due to gravity, magnetic field strength, the density of nanofluid, time-dependent magnetic field, free stream temperature, thermophoretic diffusion, and coefficient of thermal diffusion, while the density of conjugating nanoparticles is given as ρ_p for self-propelling microorganisms having a density of ρ_m with free stream N_∞. we, T, C, D_B, b, kr, and E_a are the speed of the swimming cells, the temperature, nanoparticle concentration, Brownian motion diffusion, the chemotaxis, chemical reaction, and the activation energy, respectively.

For the energy equation, the radiative heat flux approximated by the Rosseland model is employed in this study. Now, consider that the existence trivial of thermal gradient within the flow regime is small such that T^4 may be computed directly dependent on the function T_∞. The Taylor series expansion could explicitly expand T^4 while the trivial contribution of higher-order terms decimates about T_∞.

$$T^4 = 4T_\infty^4 T - T_\infty^4. \tag{9}$$

The radiative heat flux reduces to equation (10) with the invocation of the approximation of Rosseland as follows:

$$q_r = -\frac{4\sigma_e}{3ke}\frac{\partial T^4}{\partial y}, \tag{10}$$

where σ_e and ke are the Stefan-Boltzmann constant and the coefficient of mean absorption, respectively. The following transformation variables are applied to simplify the governing equations:

$$\xi = \sqrt{\frac{\Omega}{\nu(1-\mathrm{at})}}z,$$

$$u = \frac{r\Omega}{1-\mathrm{at}}F'(\xi),$$

$$v = \frac{r\Omega}{1-\mathrm{at}}G(\xi),$$

$$w = -\left(\frac{\nu\Omega}{1-\mathrm{at}}\right)^{1/2}F(\xi),$$

$$h(t) = \beta\sqrt{\frac{\nu(1-\mathrm{at})}{\Omega}},$$

$$C = C_0 - C_{\mathrm{ref}}\frac{\Omega r^2}{\nu(1-\mathrm{at})^{3/2}}\phi,$$

$$N = N_0 - N_{\mathrm{ref}}\frac{\Omega r^2}{\nu(1-\mathrm{at})^{3/2}}\chi,$$

$$T = T_0 - T_{ref}\frac{\Omega r^2}{\nu(1-\mathrm{at})^{3/2}}\theta. \tag{11}$$

Implementing the above variable on governing equations (1)–(6) subject to (7) and (8), we obtain the following:

$$\left(1 + \Lambda_1\theta\right)\left(1 + \frac{1}{\beta}\right)F''' + \Lambda_1\left(1 + \frac{1}{\beta}\right)\theta'F'' - A\left(F' + \frac{\xi}{2}F''\right) -$$

$$We\left[\xi A\left(F'F'' - GgG' - 2FF'''\right) - 4FF'F'' + 4\left(F^2F''' - FGG'\right) + A^2\left(2F' + \frac{7}{4}\xi F'' + \frac{\xi^2}{4}F'''\right) - \left(F'\right)^2 + A\left(2F'^2 - 2G^2 - 3FF''\right)\right] \tag{12}$$

$$+G^2 + 2FF'' - M\left(F' + We\left(AF' + \frac{\xi}{2}AF'' - 2FF''\right)\right) + \gamma\theta - Gr\phi - Gc\chi,$$

$$\left(1 + \Lambda_1\theta\right)G'' + \Lambda_1\theta'G' - M\left(G + We\left(AG + \frac{1}{2}\xi AG' - 2FG'\right)\right) - A\left(\frac{\xi}{2}G' + G\right)$$

$$- 2F'G + FG' - We\left[A\left(\frac{1}{4}\xi^2G'' + 2G + \frac{7}{4}\xi G'\right) + \xi A\left(F'G' + F''G - 2FG'\right) + A\left(4F'G - 3FG'\right)\right] \tag{13}$$

$$- 2FG'F' - 2GF''F - G^3 + F^2G'' = 0,$$

$$\left(\frac{(1 + \Lambda_2\theta) + R}{\mathrm{Pr}}\right)\theta'' + \Lambda_2\left(\theta'\right)^2 + D_0\mathrm{Pr}\phi'' - ME c\mathrm{Pr}\left(F'^2 + G^2\right) - \Delta\theta$$

$$+ \mathrm{Pr}Ec Fn^2 - A\left(\theta' + \frac{3}{2}\theta\right) - 2\theta F' + F\theta' + \mathrm{Pr}\left[Nt\theta'^2 + Nb\theta'\phi'\right] = 0, \tag{14}$$

$$\phi + 2Le\mathrm{Pr}\left(F\phi' - F'\phi\right) - \frac{1}{2}Le\mathrm{Pr}\left(3\phi + \xi\phi'\right)A + \frac{Nt}{Nb}\theta'' + S_0\theta''$$

$$- Le\mathrm{Pr}\sigma^{**}(1 + \delta\theta)^n\phi\,\exp\left(-\frac{E}{1 + \delta\theta}\right) = 0, \tag{15}$$

$$\chi'' - \frac{1}{2}L_b\left(3\chi + \xi\chi'\right)A + L_bF\chi' - Pe\left(\phi''\left(\chi + N\right) + \chi'\phi'\right) = 0, \tag{16}$$

subject to the constraints with respect to the similarity variable formulated in accordance with [65]:

$$F(\eta) = 0,$$

$$G(\eta) = 1,$$

$$F'(\eta) = \alpha,$$

$$\theta'(\eta) = 0, \qquad (17)$$

$$\phi(\eta) = 1,$$

$$\chi(\eta) = 1,$$

$$\text{at } \eta = 0,$$

$$F'(\eta) \longrightarrow 0,$$

$$F(\eta) \longrightarrow \frac{A\beta}{4},$$

$$\theta'(\eta) \longrightarrow 0, \qquad (18)$$

$$\phi'(\eta) \longrightarrow 0,$$

$$\chi'(\eta) \longrightarrow 0,$$

$$\text{as } \eta \longrightarrow \infty.$$

The parameters encountered in this study are defined as follows:

$$\Lambda = bT_{ref}\frac{\Omega r^2}{\nu(1 - \text{at})^{3/2}},$$

$$A = \frac{a}{\Omega},$$

$$\text{We} = \frac{\lambda_1 \Omega}{1 - \text{at}},$$

$$M = \frac{\sigma B_0^2}{\Omega \rho_f},$$

$$\gamma = \frac{(1 - \text{at})^2 \beta^* g (1 - C_\infty)(T_w - T_\infty)}{r\Omega^2},$$

$$Gr = \frac{(\rho_p - \rho_f)(C_w - C_\infty)}{\beta^* \rho_f (1 - C_\infty)T_\infty},$$

$$Gc = \frac{\gamma^*(\rho_m - \rho_f)(N_w - N_\infty)}{\beta \rho_f (1 - C_\infty)T_\infty},$$

$$\alpha = \frac{c}{\Omega},$$

$$\theta_0 = \frac{T_s}{T_0},$$

$$R = \frac{4\sigma_e T_0^3}{kke},$$

$$Nb = \frac{D_B \tau (C_w - C_\infty)}{\alpha},$$

$$\text{Pr} = \frac{\nu}{\alpha},$$

$$Nt = \frac{D_T \tau (T_w - T_\infty)}{T_\infty \alpha},$$

$$Le = \frac{\alpha}{D_B},$$

$$E = \frac{E_a}{K_1 T_0},$$

$$Ec = \frac{\nu^2}{c_p (T_s - T_0)},$$

$$Lb = \frac{\nu}{D_m},$$

$$Pe = \frac{bwe}{D_m},$$

$$N = \frac{N_\infty}{N_w - N_\infty}, \qquad (19)$$

where $\Lambda, A, We, M, \gamma, Gr, Gc, \alpha, \theta_0, R, Nb, \text{Pr}, Nt, Le, E, Ec, Lb, Pe,$ and N are the variable viscosity, unsteady parameter, Deborah number, magnetic term, mixed convection parameter, buoyancy parameter, Rayleigh number, radiation parameter, Brownian motion parameter, thermophoresis parameter, Prandtl number, Lewis parameter, Arrhenius number, Eckert number, bioconvective Lewis parameter, Peclet parameter, and bioconvective term.

2.2. Spectral Relaxation Method. Recently, the spectral homotopy analysis method is becoming a popular approach directed at solving partial differential equations largely because of the robustness and accuracy of the scheme. Significantly, the contribution of Motsa et al. in the development of this technique has sustained appreciable patronage by researchers in the field of computational fluid mechanics. The author found SHAM as a convenient and efficient scheme as it obliterates the need for ergodicity while permitting an expanse of linear cum nonlinear operators in the solution protocol. The SHAM technique demands that the design of the algorithm should be leveraged on linear operators such that numerical solutions can be added to intricate partial differential equations. The execution of SHAM invites schemes of the standard protocol, specifically convergence-controlling indices, in the attempt to lighten the constraints associated with the implementation of the traditional Homotopy analysis method [66–69]. The report of Abdelmalek et al. employed SHAM to solve higher-order Fredholm-type integrodifferential problems [70, 71]. Makukula applied SHAM to study MHD flow restrictions over a stretching surface, while the study in [72] explored SHAM to investigate bioconvection in plasma-mediated nanoparticle flow under magnetic field exposure.

Numerical computing was implemented using a special scheme of the homotopy analysis method known as spectral relaxation techniques (SRM) because it is capable of providing an elaborate description of pertinent transport parameters within the spatial domain of the rotating disc. The choice of SRM informed by its capability of multistage relaxation and robust handling of nonlinear coupled differential equations [73]. Moreover, the compactness of matrices generated is a precursor for higher accuracy of computation in a well-coupled system of equations. The method employs the concept of the Gauss-Siedel relaxation technique to decouple the system of equations. The decomposed equations are discretized and implemented by the Chebyshev pseudo-spectral method. The linear terms in the resulting equations are computed at $r+1$ while the nonlinear terms are at r. Implementing the procedure of SRM into the system of equations, we obtain the following:

$$\left(1 + \frac{1}{\beta}\right)f'''_{r+1} + a_{1,r}f''_{r+1} + a_{2,r}f''_{r+1} - Af'_{r+1} - A\frac{\xi}{2}f''_{r+1} + a_{3,r}f''_{r+1} + a_{4,r} + a_{5,r}f'''_{r+1} + a_{6,r} - 2WeA^2 f'_{r+1} - \frac{7}{4}We\xi f''_{r+1} - We\frac{\xi^2}{4}f'''_{r+1} + a_{7,r}$$

$$+ a_{8,r}f'_{r+1} + a_{9,r}f''_{r+1} + a_{10,r} + a_{11,r}f''_{r+1} - Mf'_{r+1} - MWeAf'_{r+1} - AM\frac{\xi}{2}f''_{r+1} + a_{12,r}f''_{r+1} + a_{13,r} = 0,$$

$$(20)$$

$$G''_{r+1} + b_{1,r}G''_{r+1} + b_{2,r}G'_{r+1} - MG_{r+1} - WeAMG_{r+1} - \frac{1}{2}\xi AMG'_{r+1} + b_{3,r}G'_{r+1}$$

$$- \frac{\xi}{2}AG'_{r+1} - AG_{r+1} + b_{4,r}G_{r+1} + b_{5,r}G'_{r+1} - \frac{1}{4}WeA\xi^2 G''_{r+1} - 2WeG_{r+1}$$

$$- \frac{7}{4}\xi WeG'_{r+1} + b_{6,r}G'_{r+1} + b_{7,r}G_{r+1} + b_{8,r}G'_{r+1} + b_{9,r}G'_{r+1},$$

$$(21)$$

$$\left(1 + \frac{4}{3}R\right)\theta''_{r+1} + \Lambda_1\theta'_{r+1} + c_{1,r} + c_{2,r} - \Delta\theta_{r+1} - A\theta'_{r+1} - \frac{3}{2}A\theta_{r+1}c_{3,r}\theta_{r+1} + c_{4,r}\theta'_{r+1} + c_{5,r} + c_{6,r}\theta'_{r+1} = 0, \qquad (22)$$

$$\phi''_{r+1} + d_{1,r}\phi'_{r+1} + d_{2,r}\phi_{r+1} - 0.5ALePr\xi\phi'_{r+1} + d_{3,r} - 1.5ALePr\phi_{r+1} + d_{4,r}\phi_{r+1} = 0, \qquad (23)$$

$$\chi''_{r+1} - 1.5AL_b\chi_{r+1} - 0.5AL_b\xi\chi'_{r+1} + e_{1,r}\chi'_{r+1} + e_{2,r}\chi_{r+1} + e_{3,r} + e_{4,r}\chi'_{r+1} = 0, \qquad (24)$$

subject to the boundary constraints as follows:

$$\begin{aligned} Ff_{r+1}(0) &= 0, \\ G_{r+1}(0) &= 1, \\ f'_{r+1}(0) &= \alpha, \\ \theta_{r+1}(0) &= 1, \\ \phi_{r+1}(0) &= 1, \\ \chi_{r+1}(0) &= 1, \end{aligned} \qquad (25)$$

$$\begin{aligned} f'_{r+1}(\infty) &\longrightarrow 0, \\ f_{r+1}(\infty) &\longrightarrow \frac{A}{4}\beta, \\ \theta_{r+1}(\infty) &\longrightarrow 0, \\ \phi_{r+1}(\infty) &\longrightarrow 0, \\ \chi_{r+1}(\infty) &\longrightarrow 0, \end{aligned} \qquad (26)$$

where all coefficient parameters are defined as follows:

$$a_{1,r} = \Lambda\left(1 + \frac{1}{\beta}\right)\theta_r,$$

$$a_{2,r} = \Lambda\left(1 + \frac{1}{\beta}\right)\theta'_r,$$

$$a_{3,r} = -We\xi Af'_{r+1},$$

$$a_{5,r} = 2We\xi Af_r,$$

$$a_{6,r} = 4Wef_rf'_{r+1}f'' - 4Wef_r^2 f'''_{r+1} + 4WeG - rG'_{r+1}f'_{r+1},$$

$$a_{4,r} = We\xi AG_rG'_r,$$

$$a_{7,r} = 2WeG_r^2,$$

$$a_{8,r} = -2WeAf'_{r+1},$$

$$a_{9,r} = 3WeAf_r,$$

$$a_{10,r} = f'^2_r + G_r^2,$$

$$a_{11,r} = 2f_r,$$

$$a_{12,r} = -2Mf_r,$$

$$a - 13, r = \gamma - Nr\phi_r - Nc\chi_r,$$

$$b_{1,r} = \Lambda\theta_r,$$

$$b_{2,r} = \Lambda\theta'_r,$$

$$b_{3,r} = 2Mf_{r+1},$$

$$b_{4,r} = -2f'_{r+1},$$

$$b_{5,r} = f_{r+1},$$

$$b_{6,r} = -We\xi Af'_{r+1},$$

$$b_{7,r} = -We\xi Af''_{r+1},$$

$$b_{8,r} = -4WeAf'_{r+1},$$

$$\cdot b_{9,r} 3WeAf_{r+1}$$

$$b_{10,r} = -2f_{r+1}f'_{r+1},$$

$$b_{11,r} = -2f_{r+1}f''_{r+1},$$

$$b_{12,r} = -G^3_{r+1},$$

$$b_{13,r} = f^2_{r+1},$$

$$c_{1,r} = Do\,\mathrm{Pr}\phi''_{r+1},$$

$$c_{2,r} = -MEc\mathrm{Pr}f'^2_{r+1} - MEc\mathrm{Pr}G62_{r+1} + Ec\mathrm{Pr}F''^2_{r+1},$$

$$c_{3,r} = -2f'_{r+1},$$

$$c_{4,r} = f_{r+1},$$

$$c_{5,r} = \mathrm{Pr}Nt\theta'^2_{r+1},$$

$$c_{6,r} = \mathrm{Pr}Nb\phi'_{r+1},$$

$$d_{1,r} = 2Le\mathrm{Pr}f_{r+1},$$

$$d_{2,r} = -2Le\mathrm{Pr}f'_{r+1},$$

$$d_{3,r} = \frac{Nt}{Nb}\theta''_{r+1},$$

$$e_{1,r} = L_b f_{r+1},$$

$$e_{3,r} = -PeN\phi''_{r+1},$$

$$e_{4,r} = -Pe\phi'_{r+1},$$

$$d_{4,r} = -Le\mathrm{Pr}\sigma^{**}\left(1 + \delta\theta_{r+1}\right)^n \exp\left(-\frac{E}{1 + \delta\theta_{r+1}}\right),$$

$$e_{2,r} = -Pe\phi'_{r+1}.$$

$$(27)$$

The Gauss-Lobatto collocation points define the unknown functions as follows:

$$\xi_j = \cos\left(\frac{\pi j}{N}\right), \quad j = 0, 1, 2, \ldots, N; \; 1 \le \xi \le -1, \qquad (28)$$

where N is the number of collocation points. The domain of the physical region $[0, \infty)$ is simplified into $[-1, 1]$. Hence, the problem is solved on the interval of $[0, L]$ and not $[0, \infty)$. Here, the following transformation to map the interval is used:

$$\frac{\eta}{L} = \frac{\xi + 1}{2}, \quad -1 \le \xi \le 1, \qquad (29)$$

where L represents the scaling parameter used in implementing the boundary constraints at infinity. The following initial approximation is chosen to satisfy the boundary conditions in equations (17) and (18)as follows:

$$f_0(\eta) = \alpha\left(e^{-\eta} + 1\right),$$
$$\theta_0 = \phi_0 = G_0 = e^{-\eta}. \qquad (30)$$

The choice of SRM in this study is due to its elegance and easy computations. This method has been proven novel in the literature. The system of equations (22)–(24) can be solved iteratively for the unknown functions starting from the initial approximations in (29). The iteration protocols are presented for $u_{r+1}(y, t), \vartheta_{r+1}(y, t)$, and $\varphi_{r+1}(y, t)$ when $r = 0, 1, 2$. To solve the system of equations (22)–(24), the equations are discretized with the help of the Chebyshev spectral collocation method in the $y-$ coordinate while the $t-$ component is derived over the implicit scheme of the finite differencing method. This numerical approach is used with the centre about a midpoint between t^{n+1} and t^n. The midpoint is expressed as follows:

$$t^{n+(1/2)} = \frac{t^{n+1} + t^n}{2}. \qquad (31)$$

About the centroid $t^{n+(1/2)}$ to the undisclosed functions, say $u(y, t), \vartheta(y, t)$, and $\varphi(y, t)$ and analogous terms reduce to

$$u\left(y_j, t^{n+(1/2)}\right) = u_j^{n+(1/2)} = \frac{u_j^{n+1} + u_j^n}{2},$$

$$\left(\frac{\partial u}{\partial t}\right)^{n+(1/2)} = \frac{u_j^{n+1} - u_j^n}{\Delta t},$$

$$\vartheta\left(y_j, t^{n+(1/2)}\right) = \vartheta_j^{n+(1/2)} = \frac{\vartheta_j^{n+1} + \vartheta_j^n}{2},$$

$$\left(\frac{\partial \vartheta}{\partial t}\right)^{n+(1/2)} = \frac{\vartheta_j^{n+1} - \vartheta_j^n}{\Delta t},$$

$$\varphi\left(y_j, t^{n+(1/2)}\right) = \varphi_j^{n+(1/2)} = \frac{\varphi_j^{n+1} + \varphi_j^n}{2},$$

$$\left(\frac{\partial \varphi}{\partial t}\right)^{n+(1/2)} = \frac{\varphi_j^{n+1} - \varphi_j^n}{\Delta t}.$$

$$(32)$$

An important role of the collocation scheme is to employ the differentiation matrix D to invoke approximation operation on the derivative of the required derivatives, which are specified as follows:

$$\frac{d^r u}{dy^r} = \sum_{k=0}^{N} D_{ik}^r u(\xi_k) = D^r u, \quad i = 0, 1, \ldots N,$$

$$\frac{d^r \vartheta}{dy^r} = \sum_{k=0}^{N} D_{ik}^r \vartheta(\xi_k) = D^r \vartheta, \quad i = 0, 1, \ldots N, \qquad (33)$$

$$\frac{d^r \varphi}{dy^r} = \sum_{k=0}^{N} D_{ik}^r \varphi(\xi_k) = D^r \varphi, \quad i = 0, 1, \ldots N,$$

subject to (25) and (26) where we get the following:

$$u_{r+1} = \begin{bmatrix} u_{r+1}(x_0, t) \\ u_{r+1}(x_1, t) \\ \vdots \\ u_{r+1}(x_{N_{x-1}}, t) \\ u_{r+1}(x_{N_x}, t) \end{bmatrix},$$

$$a_{0,r} = \begin{bmatrix} a_{0,r}(x_0, t) \\ & a_{0,r}(x_1, t) \\ & & \ddots \\ & & & \ddots \\ & & & & a_{0,r}(x_{N_x}, t) \end{bmatrix},$$

$$\vartheta_{r+1} = \begin{bmatrix} \vartheta_{r+1}(x_0, t) \\ \vartheta_{r+1}(x_1, t) \\ \vdots \\ \vartheta_{r+1}(x_{N_{x-1}}, t) \\ \vartheta_{r+1}(x_{N_x}, t) \end{bmatrix},$$

$$b_{0,r} = \begin{bmatrix} b_{0,r}(x_1, t) \\ & b_{0,r}(x_2, t) \\ & & \ddots \\ & & & \ddots \\ & & & & b_{0,r}(x_{N_x}, t) \end{bmatrix}, \qquad (34)$$

$$\varphi_{r+1} = \begin{bmatrix} \varphi_{r+1}(x_0, t) \\ \varphi_{r+1}(x_1, t) \\ \vdots \\ \varphi_{r+1}(x_{N_{x-1}}, t) \\ \varphi_{r+1}(x_{N_x}, t) \end{bmatrix},$$

$$c_{0,r} = \begin{bmatrix} c_{0,r}(x_0, t) \\ & c_{0,r}(x_1, t) \\ & & \ddots \\ & & & \ddots \\ & & & & c_{0,r}(x_{N_x}, t) \end{bmatrix}.$$

The same diagonal matrix goes for $a_{1,r}, a_{2,r}, b_{1,r}, b_{2,r}, b_{3,r}, b_{4,r}, c_{0,r}$, and $c_{1,r}$.

$$N_1 u_{r+1}^{n+1} = H_1 u_{r+1}^n + G_1,$$
$$N_2 \vartheta_{r+1}^{n+1} = H_2 \vartheta_{r+1}^n + G_2, \qquad (35)$$
$$N_3 \varphi_{r+1}^{n+1} = H_3 \varphi_{r+1}^n + G_3.$$

The equations are susceptible to these initial conditions and boundary conditions as follows:

$$u_{r+1}(xN_x, t^n) = \vartheta_{r+1}(xN_x, t^n) = \varphi_{r+1}(xN_x, t^n) = 0,$$
$$u_{r+1}(x_0, t^n) = 1,$$
$$\vartheta_{r+1}(x_0, t^n) = \varphi_{r+1}(x_0, t^n) = 1 + v e^{nt}, \quad n = 1, 2, \ldots,$$
$$u_{r+1}(y_j, 0) = e^{-y_j},$$
$$\vartheta_{r+1}(y_j, 0) = \varphi_{r+1}(y_j, 0) = e^{-y_j} + o' e^{nt}.$$
$$(36)$$

2.3. Computational Data. The array of important thermophysical quantities such as skin friction, Nusselt number, and Sherwood number parameters serving as input data for computational investigation is contained for selected dimensionless variables and is illustrated in Table 1. Computational values of skin friction, Nusselt number, and Sherwood number for key flow parameters are described in Table 2.

3. Validation of Results

The convergence and accuracy of the present study are verified by comparing the results from the investigation with the published reports of Abdelmalek et al. [64] when $\Lambda_1 = \beta = \Lambda_2 = Do = \Delta = 0$ at variable viscosity and thermal conductivity. The comparison was conducted for $A = 1.5, 1.7, 1.9$, $M = 0.1, 0.4, 0.7$, and $Gr = 0.2, 0.4, 0.8$ as shown in Tables 3 and 4. The present study results agree with the literature data with high accuracy in the numerical computing procedure implemented in this work. Therefore, these outcomes motivated the study of the effects of other flow parameters on the complex nanofluid-mediated bacterium-plasma fluid.

4. Results and Discussion

The set of transformed coupled third-order ordinary differential equations described in equations (12)–(16) and the boundary conditions expressed in equations (17) and (18) were solved numerically using the spectral relaxation method (SRM). The contribution of changes in the various critical parameters on velocity $(1 + (1/\beta))f'(\eta)$, azimuthal velocity component $G(\eta)$, temperature distribution $\theta(\eta)$, and concentration distribution $\phi(\eta)$ are given in a diagrammatic form while the Nusselt number, Sherwood number, and skin friction are computed and tabulated. All key parameters plotted are obtained by setting other parameters at constant values as follows:

Table 1: Computational values of skin friction, Nusselt number, and Sherwood number for key flow parameters.

β	We	M	Gr	Gc	A	R	Pr	$-f''(0)$	$-g'(0)$	$-\theta'(0)$	$-\phi'(0)$
1.0								1.1621	0.1639	1.0048	1.0564
2.0								1.1867	0.9065	1.0076	1.0595
3.0								1.2107	1.1721	1.0104	1.0627
	0.2							1.1254	1.4417	1.0416	1.1165
	0.3							1.1544	1.5509	1.0452	1.1215
	0.4							1.1843	1.6635	1.0488	1.1267
		0.4						2.4309	1.5260	1.0996	1.2462
		0.7						2.4062	1.3608	1.0996	1.2462
		0.5						2.4024	1.2251	1.0996	1.2462
			0.2					1.6309	1.8406	1.3958	1.3410
			0.4					1.0652	1.8919	1.3958	1.3410
			0.6					2.0039	1.9990	1.3958	1.3410
				0.3				1.2314	1.8014	1.0081	1.0743
				0.5				1.2574	1.6118	1.0112	1.0743
				0.7				1.2830	1.4244	1.0142	1.0743
					0.1			1.3076	1.2918	1.0792	1.6564
					0.3			1.3353	1.3914	1.0838	1.6564
					0.5			1.3628	1.4981	1.0886	1.6564
						0.5		1.8774	2.6832	2.0824	2.8987
						1.0		1.9132	2.6757	2.0876	2.8987
						2.0		1.9499	2.1516	2.0931	2.8987
							0.71	2.1906	1.6775	2.1223	1.2273
							3.00	2.1433	1.7063	2.1151	1.2273
							7.00	1.0978	1.7409	2.1083	1.2273

Table 2: Computational values of skin friction, Nusselt number, and Sherwood number for key flow parameters II.

Ec	Nt	Nb	So	Do	Pe	$-f''(0)$	$-g'(0)$	$-\theta\prime(0)$	$-\phi\prime(0)$	$-\chi\prime(0)$
0.01						1.6145	1.3575	1.9599	1.3254	1.6145
0.05						1.6264	1.3612	1.9601	1.3254	1.6145
0.10						1.6288	1.3653	1.9666	1.3254	1.6145
	0.2					1.1621	1.1639	1.0104	1.2702	1.1266
	0.4					1.1867	1.9065	1.0048	1.2702	1.8900
	0.6					1.2107	1.9474	1.0076	1.2702	1.9995
		0.2				1.5452	1.0382	1.1237	1.4355	1.1980
		0.5				1.5676	1.7577	1.1294	1.4575	1.4577
		0.8				1.5903	1.8895	1.1353	1.4791	1.6940
			0.5			1.5732	1.1222	1.7285	1.2045	1.6198
			1.0			1.5963	1.2471	1.7285	1.2661	1.6198
			2.0			1.6198	1.3906	1.7285	1.2741	1.6198
				0.3		2.4548	2.5944	2.0957	2.3635	2.0419
				0.6		2.4764	2.7815	2.1019	2.6159	2.0419
				0.9		2.4981	2.9805	2.1082	2.8718	2.0419
					0.3	1.5586	1.7213	1.9097	1.7668	1.1460
					0.5	1.5805	1.8465	1.9097	1.8134	1.3180
					0.7	1.6026	1.9885	1.9097	1.8604	1.5033

Table 3: Comparison of the present study with that of Abdelmalek et al. [64] when $\beta = 1$.

Pe	Lb	Abdelmalek et al. [64] $-\chi\prime(0)$	Present study $-\chi\prime(0)$
0.1		0.5716	0.5714
0.5		0.6813	0.6811
1.0		1.7900	1.8000
	0.1	0.0328	0.0326
	0.4	1.5480	0.5476
	0.8	0.9854	0.9852

TABLE 4: Comparison of the present study with that of Abdelmalek et al. [64] when $\beta = 1$.

			[64]		Present study	
A	M	Nr	$-f''(0)$	$-g'(0)$	$-f''(0)$	$-g'(0)$
1.5			1.9986	2.5672	1.9984	2.5671
1.7			2.1149	2.6671	2.1147	2.6670
1.9			2.2282	2.7668	2.2280	2.7666
	0.1		1.7531	2.3596	1.7528	2.3597
	0.4		1.8619	2.4393	1.8613	2.4387
	0.7		1.9646	2.5168	1.9642	2.5166
		0.2	1.8696	2.4687	1.8694	2.4685
		0.4	1.8967	2.4651	1.8965	2.4649
		0.8	1.9239	2.4620	1.9237	2.4616
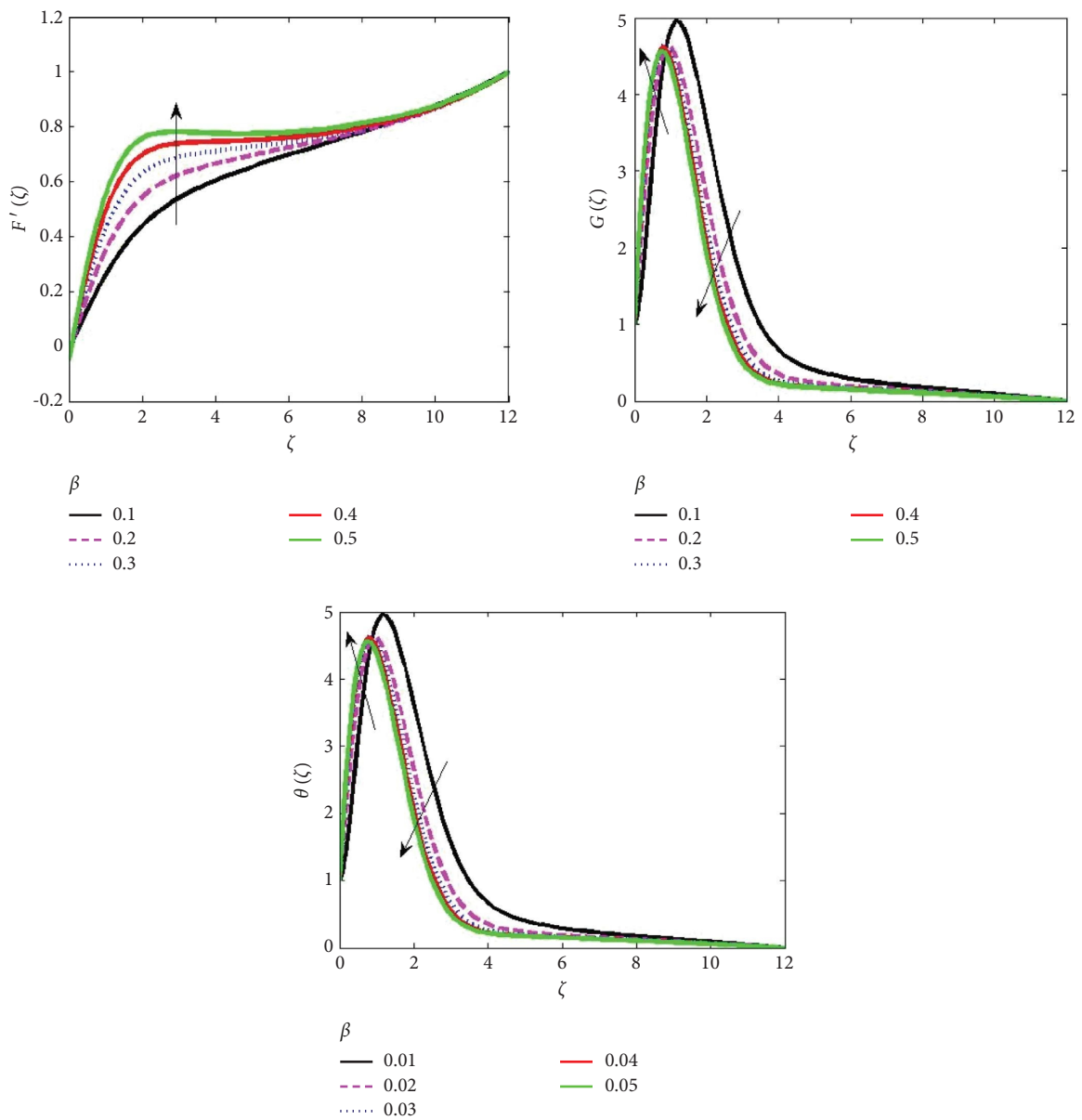
FIGURE 2: Influence of Casson parameter on the velocity, azimuthal velocity, and temperature.
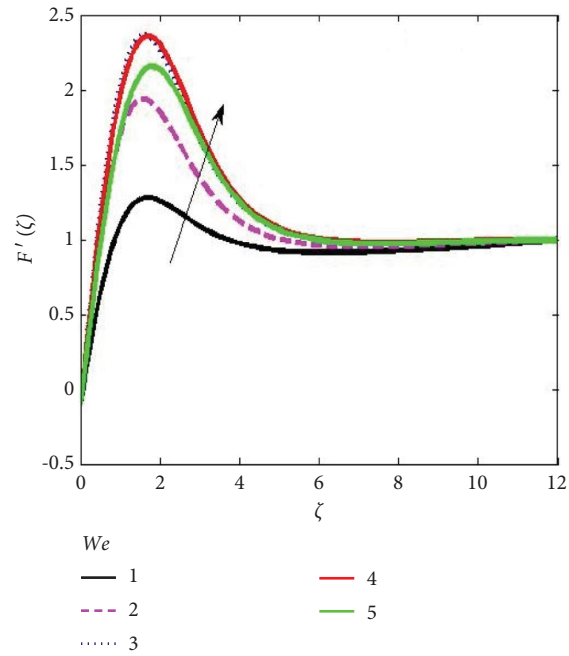
FIGURE 3: Effect of Deborah number on the velocity distribution.
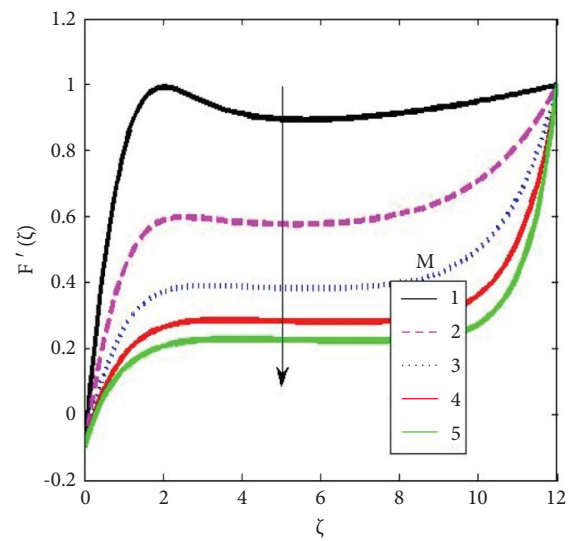
FIGURE 4: Effect of magnetic parameter on the velocity distributions.
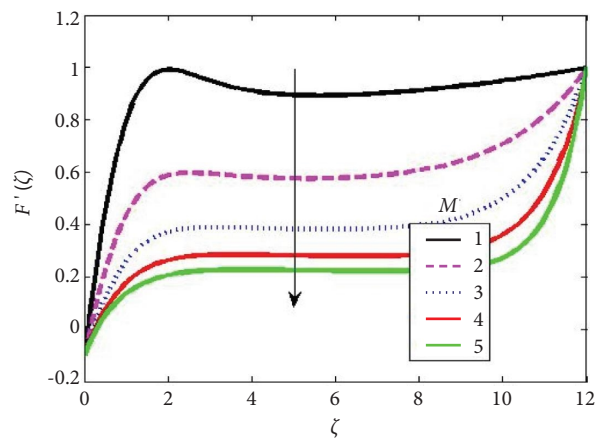
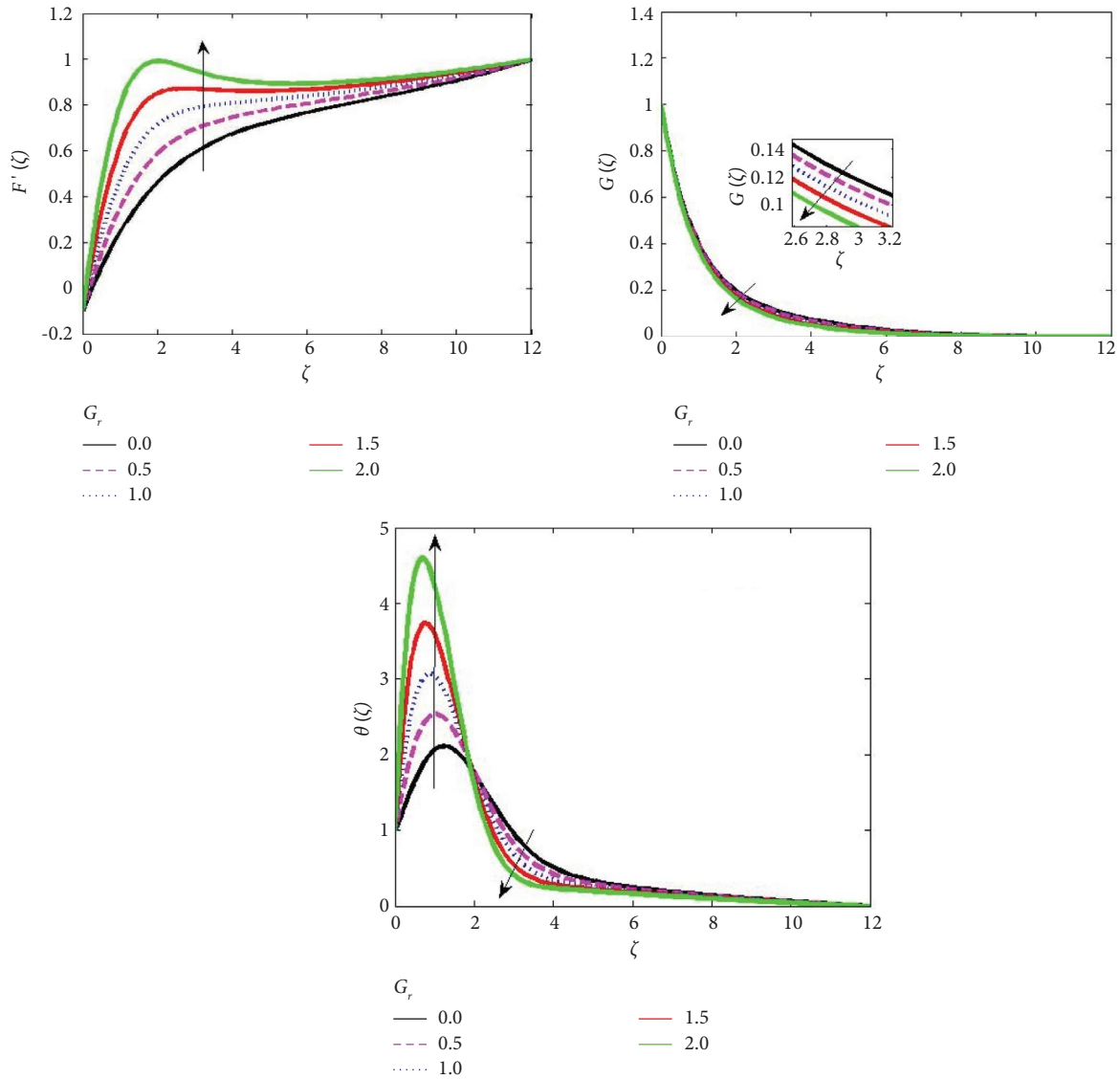FIGURE 5: Effect of unsteady parameter on the temperature distributions.

FIGURE 6: Effect of buoyancy ratio constant on the velocity, azimuthal velocity, and temperature distributions.

$$
\begin{aligned}
De &= 0.2 \\
\lambda &= 0.1, \\
Gc = A &= 0.5, \\
Gr &= 0.3, \\
\alpha &= 0.2, \\
Pr &= 0.71, \\
\sigma &= 0.2, \\
Nb &= 0.6, \\
Nt &= 0.3,
\end{aligned}
\qquad
\begin{aligned}
Lb &= 0.4, \\
E &= 0.5, \\
Pe &= 0.4, \\
M &= 1, \\
R &= 0.9, \\
Ec &= 0.01, \\
\beta &= 2.0.
\end{aligned}
\tag{37}
$$

Figure 2 shows the rheological behaviour of plasma-nanofluid is modelled after the Casson model denoted with (β), for which there is the influence of velocity distribution, azimuthal velocity, and temperature distribution.
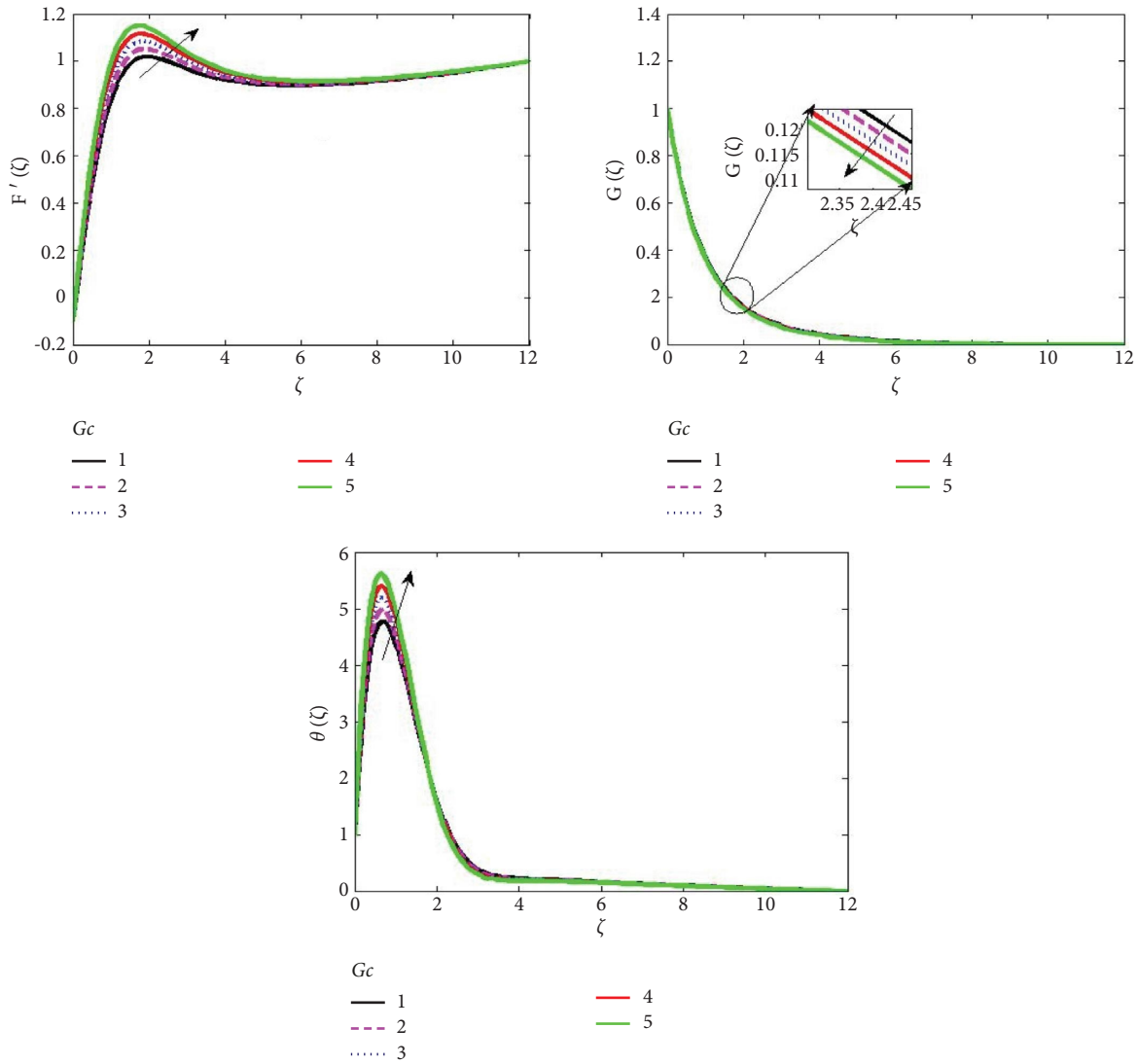
FIGURE 7: Effect of the Rayleigh number on the velocity, azimuthal velocity, and temperature.

The supposition of zero rest position translated to an increase in the value of β as an antecedent to upraise both temperature and azimuthal velocity in the wall vicinity, whereas a decrease is noticeable far from the wall of the spinning disc. On the contrary, an elevation of the velocity distribution is observed as the values of β increase. Physically, variable viscosity and thermal conductivity tend to increase the viscosity of the complex fluid in the vicinity of the rotating member but quickly degenerate in the far region of the circular plate. The result shows that growth in β parameter produces a fast movement to fluid flow within the circular disc because as β increases, the yield stress P_y of the Casson parameter increases while the quantity of plastic dynamic viscosity μ_B degenerates.

Figure 3 illustrates the effect of Deborah number (De) on the velocity distribution. An elevation of the velocity distribution is noticeable as the Deborah number (De) increases. In experiments, if De = 0, an outcome for viscous fluid is obtained, while De = 1, 2, 3, 4, and 5 shows a viscoelastic characteristic. The Deborah number explains the relaxation time to observation time ratio, which means that the peak value of De is equivalent to a large relaxation time, which prompts enhancement in velocity distribution around the velocity field.

The contribution of Hartmann number (M) on momentum transport is described in Figure 4, which shows noticeable degeneration in the velocity distribution for increasing values of M. The imposed magnetic field transversely to the electrically conducting fluid flow produces Lorentz force, which exemplified velocity drag-like that retard the momentum of a conducting plasma-mediated bacterium-containing nanofluid.

Figure 5 illustrates the impact of the unsteady parameter (A) on the temperature distribution. The unsteadiness in the fluid temperature is noticeable close to the plate as the value of the unsteady parameter increases. Physically, for a variable viscosity and thermal conductivity, random mixing of fluid particles causes their temperature to increase drastically. Figure 6 illustrates the distribution of buoyancy ratio constant (Gr) in the velocity field, azimuthal velocity, and temperature
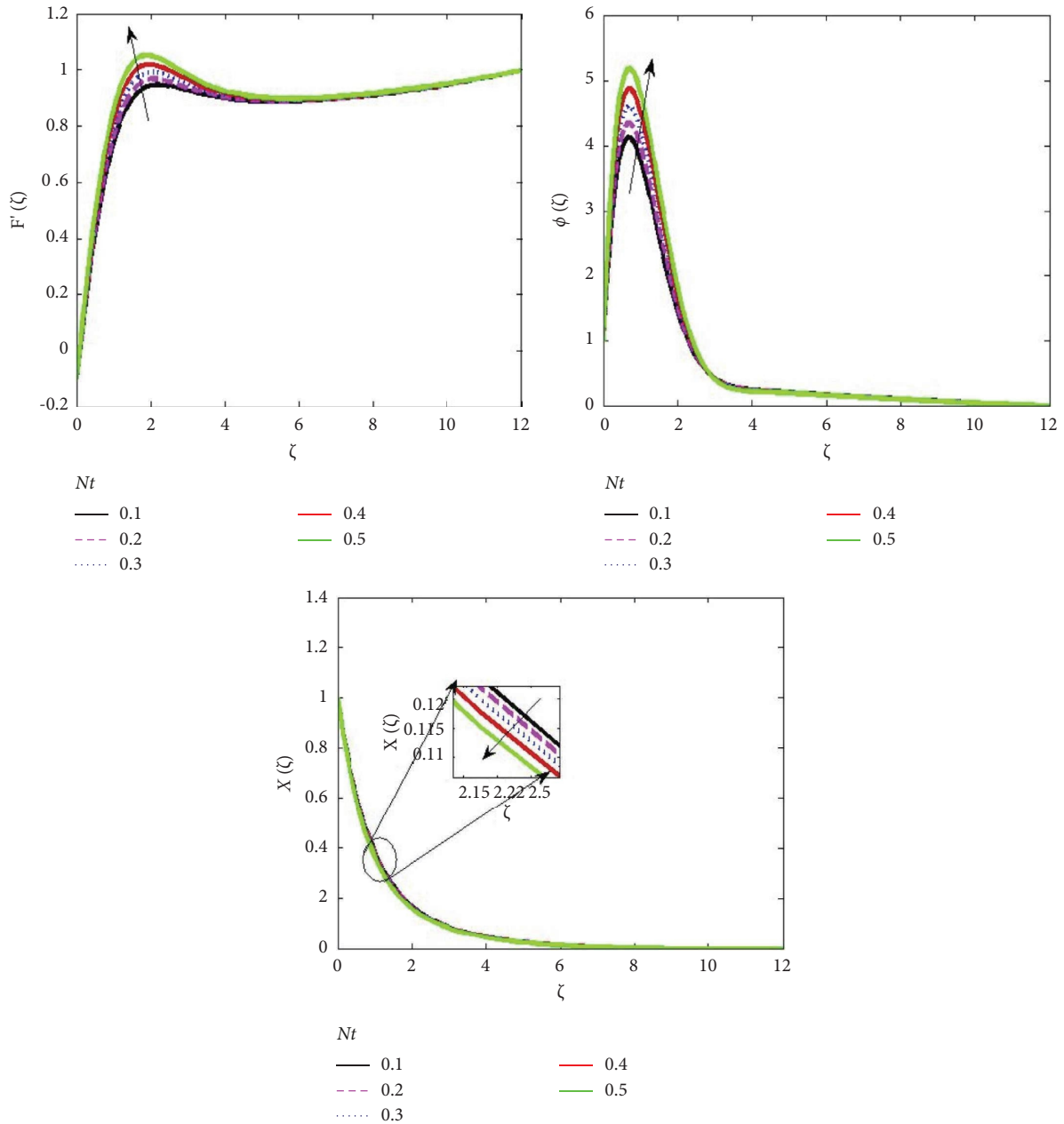
FIGURE 8: Effect of the thermophoresis parameter on the velocity, concentration, and motile density distributions.

distribution. An increase in the value of Gr is observed to degenerate the azimuthal velocity but causes a drastic increase in the velocity distribution. In addition, escalating the magnitude of Gr drastically precipitates the thermal field in the microorganism-laden fluid, especially in the neighbourhood of the rotating plate, while the fluid suffers thermal decay in the far field. The buoyancy ratio constant acts like an upward force, increasing the entire hydrodynamic boundary layer.

The competing contribution of buoyancy in the bid to induce flow by subduing friction in the vicinity of the rotating circular disc is captured in Figure 7. This distribution exhibits the impacts of the Rayleigh number on the velocity, azimuthal velocity, and temperature distribution. It was noticed that an increase in the velocity and temperature

distribution is noticeable, whereas the azimuthal velocity profile shows a downward slope for selected cases considered. Physically, it can be inferred that the Rayleigh number is greatly influenced by the buoyancy force in bioconvection analysis. Physically, it can be inferred that the Rayleigh number is greatly influenced by bouyant force in bioconvection analysis with maximum variation of Gc while the contribution of rotation field being the azimuthal velocity components becomes very weak.

Figure 8 illustrates the consequence of the thermophoresis parameter (Nt) on the velocity, concentration, and motile density distributions, respectively. An increase in the velocity and concentration distribution is noticeable in the plot because of an increase in Nt values, whereas a decrease
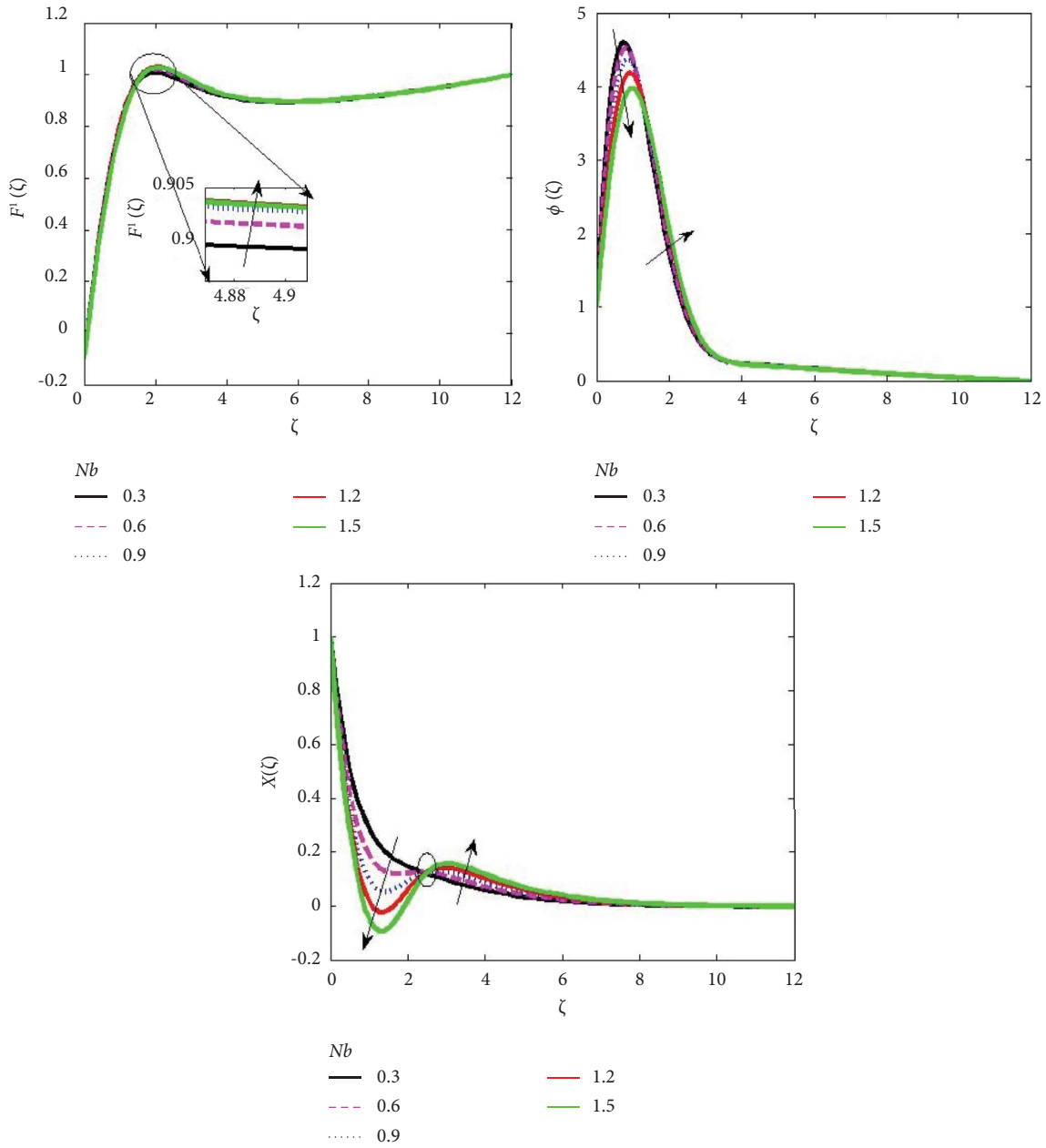
FIGURE 9: Effect of the Brownian motion parameter on the velocity, concentration, and motile density distributions.

in the motile density distribution can be observed. The impact of the Brownian motion parameter (Nb) on the velocity distribution, concentration distribution, and motile density distribution is depicted in Figure 9. As the magnitude of Nb increases, an increase in velocity distribution is noticeable which translates to an over-ridden influence of convective thermal transport within the motile-organism media under combined magnetic cum rotational force. Also, an increase in Nb causes degeneration to the concentration and motile density distribution near the plate and in the distal area from the plate. Physically, a random collision of fluid particles causes a decrease in fluid velocity; hence, an increase in Nb leads to an increase in the boundary layer in the momentum field.

The consequence of the population of motile microorganisms on convective thermal transport is captured in Figure 10. The increase in Pe causes an increase in the motile density distribution near the disc, as observed in Figure 10, whereas a degeneration is far away from the plate. Figure 11 shows the contribution of the Eckert parameter (Ec) on the velocity distribution, azimuthal velocity, and temperature distribution, respectively. The velocity alongside the temperature is noticed to increase as the Eckert number escalates. A decrease in the azimuthal velocity is noticeable with the increasing quantity of the Ec parameter. The viscous dissipation term (Eckert parameter) portrays the relationship between the flow of kinetic energy and the enthalpy, which describe energy transformation occasioned by viscous
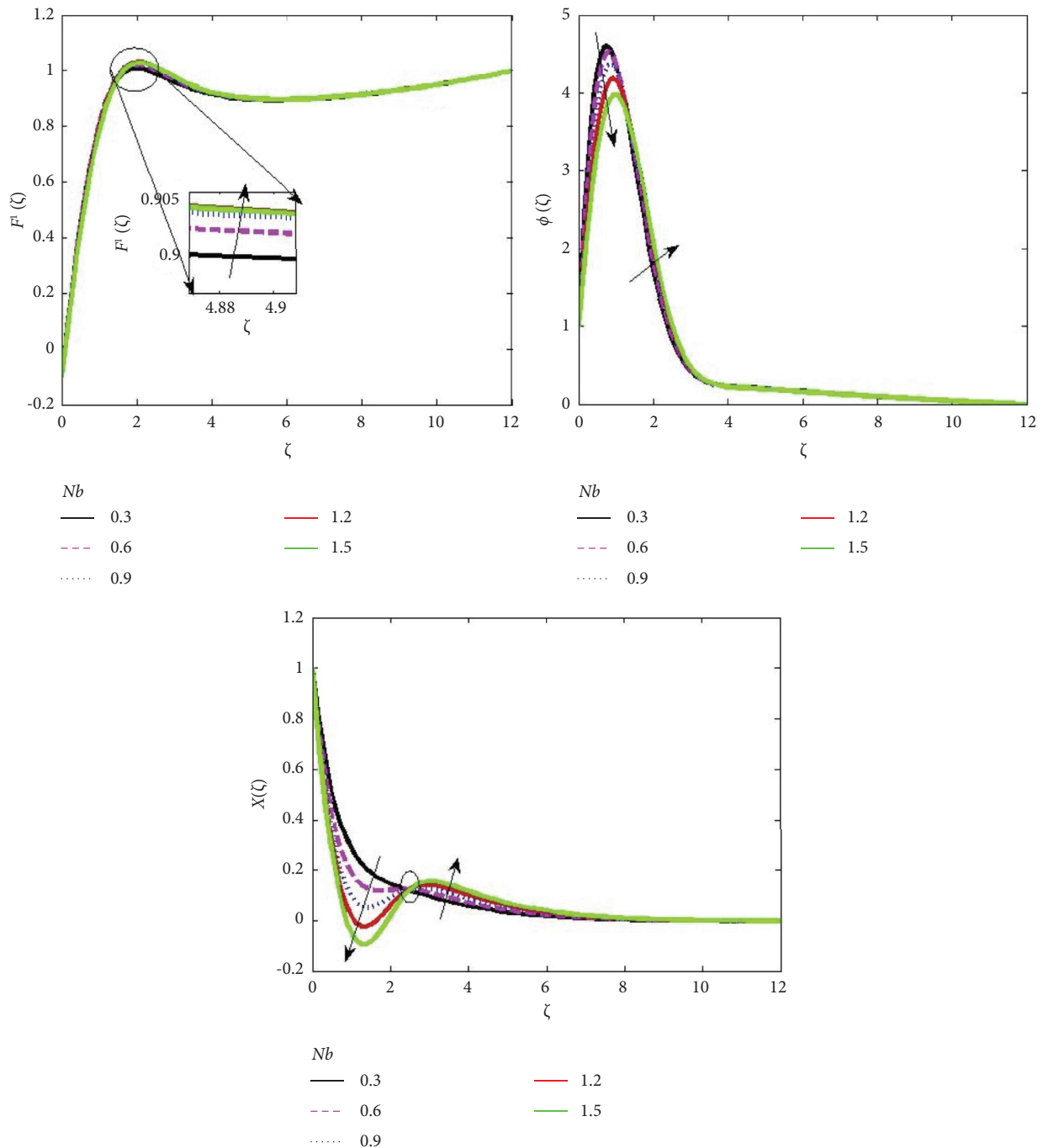
FIGURE 10: Effect of the Brownian motion parameter on the velocity, concentration, and motile density distributions.

stresses. Consequently, observed viscous dissipation mediates streamwise thermal growth in the momentum field.

Therefore, the thickness in the thermal and hydrodynamic boundary layers leads to redistribution of microorganisms within the flow stream towards the rotating member of the microfluidic setup. The effect of the radiation parameter (R) on the velocity and temperature distributions captured in Figure 12 illustrates an increase in the value of R, leading to an elevation in both velocity and temperature distributions. A nonlinear relationship between radiation and temperature was observed which is in tandem with the findings in the study of Uddin and coworkers [52]. This is true because of the random collision of fluid particles within the boundary layer. Hence, radiation is significant in as much $R > 0$ ($i.e.$, $R \neq 0$). The distribution of Prandtl number (Pr) along the thermal and momentum field in Figure 13 describes an increase in the value of Pr, which elevates the velocity and temperature distribution. Pr explains the relationship between momentum viscosity and thermal conductivity, and it coordinates the relative thickening of both momentum and thermal layers in the heat transport analysis. At lower Pr, higher thermal conductivities and thick
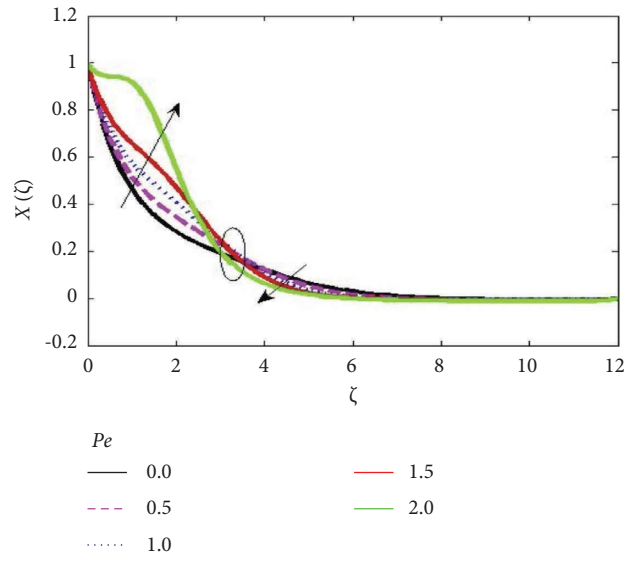
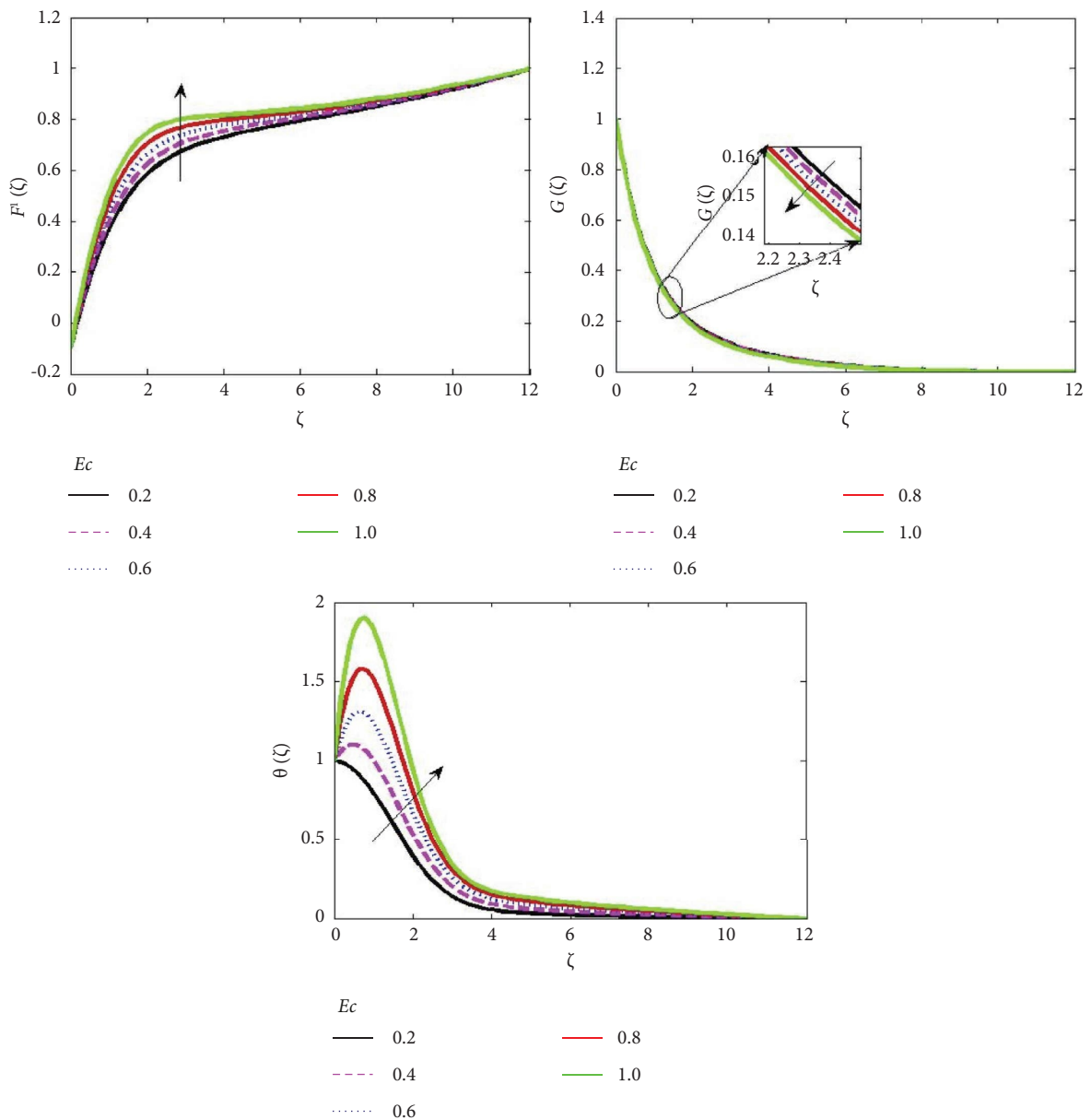FIGURE 11: Effect of the Peclet number on the motile density distribution.

FIGURE 12: Effect of the Eckert number on the velocity, azimuthal velocity, and temperature distributions.
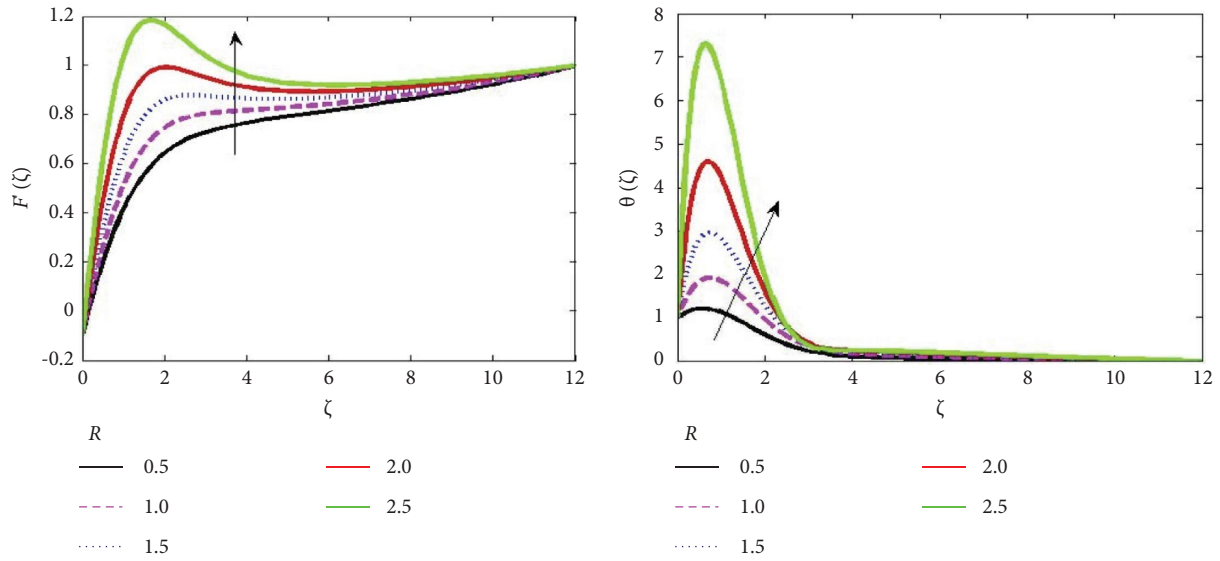
FIGURE 13: Effect of the thermal radiation parameter on the velocity and temperature distributions.
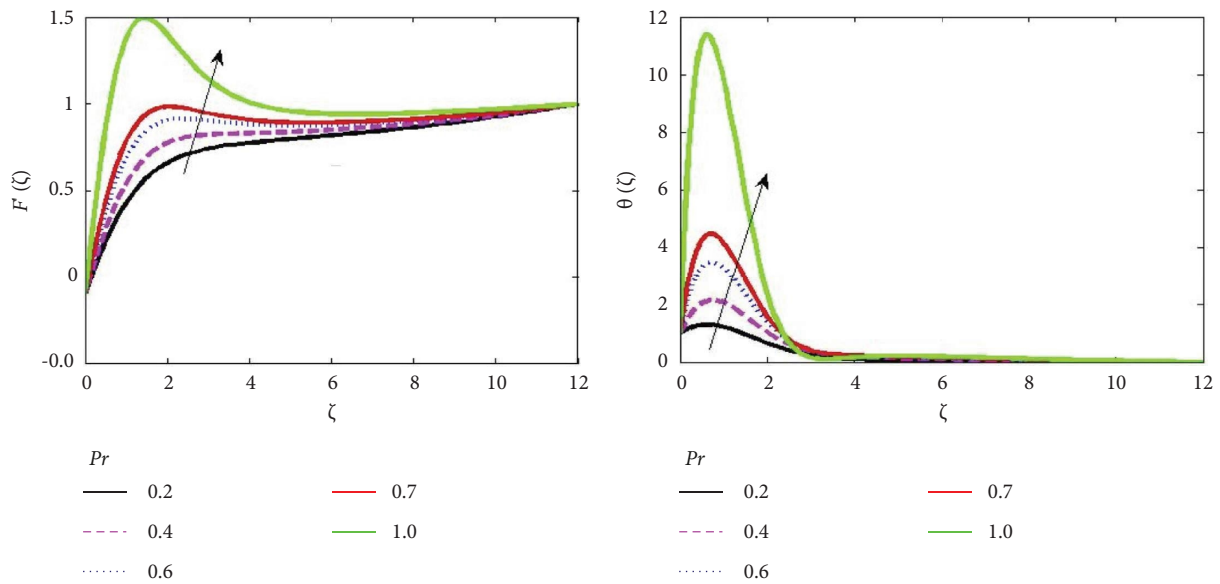

FIGURE 14: Effect of the Prandtl number on the velocity and temperature distributions.

thermal boundary layer structures give room for heat to diffuse when Pr is at the peak. Figure 14 illustrates the impact of the Prandtl parameter on the velocity field and thermal transport in the vicinity of the thermal boundary layer. The profile of this observation is in the similitude of the effect of thermal radiation parameter on momentum and temperature fields as captured in the former plot.

5. Conclusion

Analysis of fluid transportation in rotating porous microchannels with thermal and concentration impact has been discussed, emphasizing modelled plasma flow in a bacterium-containing nanofluid media. It is worth noting

that the work here focuses on the transport phenomena of fluids in a rotating porous microchannel with the effects of heat and mass transfer. This study employed similarity variables on the formulated systems of partial differential equations to obtain a set of coupled nonlinear total differential equations. The SRM is more accurate due to its easy computations than methods in the literature reviewed in this study. Therefore, the choice of SRM is due to its accuracy and elegance. Important parameters related to thermal radiation, unsteadiness, thermophoresis, Brownian motion, Eckert number, and Deborah number were discussed using graphical data. The viscosity and thermal conductivity of the fluid flow are considered to vary within the boundary layer regime. The present outcomes show that

the case of variable viscosity and thermal conductivity increases the velocity distribution due to the increase in the Casson parameter.

With the production of Lorentz force, the velocity alongside the hydrodynamic boundary layer degenerates. The viscous dissipation term (Eckert number) dramatically affects the velocity and temperature distribution, and an increase in Ec elevated the velocity and temperature fields, respectively. The unsteadiness parameter was found to cause unstable flow close to the wall and becomes normal far away from the plate where the impact of viscosity and thermal conductivity is minimal. In the analysis, the disc is assumed to be stretched with variable viscosity and thermal conductivity. However, diffusing nanoparticles are assumed to be situated at the rotating disk. The concentration of nanofluid species is taken to be high such that Soret and Dufour's contribution cannot be neglected [74].

Within the boundary layer region, the duo of thermal conductivity and viscosity of the complex fluid was observed to show ascending variation while the motile microorganisms swim peripherally over the rotating disk. Augmentation in the flow field is occasioned by the field imposition cum rotating disk that showed increase in the thermal radiation parameter which precipitates the fluid thermal condition, thus energising propulsion in the microorganism stream. We reported considerable growth in the thermal and hydrodynamic boundary layer increases is regarded as the augmentation in bacterial-embedded flow. The outcomes of this study can be a useful application in the design and development of bioreactors and microfluidic devices in varied fields of bioengineering, biomedical, and biotechnology. A future outlook of this study would be to analyse the contribution of Coriolis effect in a centrifugal microfluidics paradigm.

Nomenclature

A: Unsteadiness parameter (−)
B_0: Magnetic field strength (Tesla)
$B(t)$: Time-dependent magnetic field (Tesla)
b: Chemotaxis (m/s)
D_B: Brownian motion diffusion (1/m²s)
D_T: Thermophoretic diffusion (1/m²s)
E_a: Activation energy (J/mol)
N_∞: Free stream motile density (kg/m³)
N_s: Surface motile microorganism (−)
T_∞: Free stream temperature (K, °C)
C: Nanoparticle concentration (mol/dm³)
Cs: Surface concentration (mol/dm³)
E: Arrhenius chemical reaction parameter (−)
Ec: Eckert number (−)
Lb: Bioconvective Lewis (−)
Le: Lewis number (−)
Nb: Brownian motion parameter (−)
Nt: Thermophoresis parameter (−)
Pe: Peclet number (−)
Pr: Prandtl number (−)
Ts: Surface temperature (K, °C)
Gc: Motile density Grashof number (−)

Gr: Mass Grashof number (−)
M: Magnetic parameter (−), Hartmann number
R: Thermal radiation parameter (−)
T: Temperature (K, °C)
t: Time (s)
We: Deborah number (−)
kr: Chemical reaction (mol)
ke: Coefficient of mean absorption (−)
qr: Radiative heat flux (W/m²)
we: Speed of swimming cells (m/s)
N: Bioconvective term (m/s)
u: Velocity in the x-direction direction (m/s)
a: Coefficient parameter (unitless)
c: Nanoparticle concentration (mol/mL)
r: Chebyshev linear term (unitless)
g^*: Gravity (m/s²).

Greek Symbols

$\mu(T)$: Temperature-dependent dynamic viscosity (m²/s)
$k(T)$: Temperature-dependent thermal conductivity (W/m·K)
v: Kinematic viscosity (m²/s)
σ_e: Electrical conductivity (S/m)
β^*: Volume suspension coefficient (m³)
β: Casson parameter (unitless)
ρ_f: Nanofluid density (kg·m⁻³)
$\tau = (\rho c)_p/(\rho c)_v$: Thermal diffusion coefficient (m²/s)
ρ_p: Nanoparticle density (kg/m³)
ρ_m: Microorganisms mean density (kg/m³)
Λ_1: Variable viscosity (1/s)
Λ_2: Variable thermal conductivity (unitless)
γ: Thermal Grashof number (unitless)
Δ: Heat generation parameter (unitless)
ξ, θ_0: Rayleigh number (unitless)
Ω: Reference concentration
η: Similarity variable (unitless)
λ: Variable viscosity parameter (1/s)
α: Thermal diffusivity (m²·s⁻¹).

Subscripts/Superscripts

$*$: Superscript
0: Initial value
1: Next stage value
∞: Free stream
B: Magnetic field strength (Am⁻¹)
f: Dimensionless velocity (unitless)
m: Mean condition (unitless)
p: Condition relating to the nanoparticle or constant pressure (unitless)
Ref: Reference condition (unitless)
s: Surface condition (unitless)
T: Temperature condition (K)
v: Kinematic viscosity condition
w: Velocity component in z-direction (m/s)
γ: Thermal buoyancy force (unitless)

z: Direction of flow (unitless).

Abbreviations

CD: Circular-disc
CNT: Carbon nanotube
SWCNT: Single-walled carbon nanotubes
HAM: Homotopy analysis method
MHD: Magneto hydrodynamics
ODE: Ordinary differential equation
SHAM: Spectral homotopy analysis method
SRM: Spectral relaxation method.

Data Availability

This research is a nonfunded numerical study.

Conflicts of Interest

The authors declare that they have no conflicts of interest.

Acknowledgments

References

[1] C. Yi, C. W. Li, S. Ji, and M. Yang, "Microfluidics technology for manipulation and analysis of biological cells," *Analytica Chimica Acta*, vol. 560, pp. 1–23, 2006.

[2] T. Luo, L. Fan, R. Zhu, and D. Sun, "Microfluidic single-cell manipulation and analysis: methods and applications," *Micromachines*, vol. 10, no. 2, pp. 104–135, 2019.

[3] K. Ziółkowska, R. Kwapiszewski, and Z. Brzózka, "Microfluidic devices as tools for mimicking the in vivo environment," *New Journal of Chemistry*, vol. 35, no. 5, pp. 979–990, 2011.

[4] A. Burmeister and A. Grünberger, "Microfluidic cultivation and analysis tools for interaction studies of microbial co-cultures," *Current Opinion in Biotechnology*, vol. 62, pp. 106–115, 2020.

[5] B. C. Dhar and N. Y. Lee, "Lab-on-a-chip technology for environmental monitoring of microorganisms," *Biochip Journal*, vol. 12, pp. 173–183, 2018.

[6] S. Pinck, L. M. Ostormujof, S. Teychené, and B. Erable, "Microfluidic microbial bioelectrochemical systems: an integrated investigation platform for a more fundamental understanding of electroactive bacterial biofilms," *Microorganisms*, vol. 8, no. 1–22, p. 1841, 2020.

[7] T. S. Kaminski, O. Scheler, and P. Garstecki, "Droplet microfluidics for microbiology: techniques, applications and challenges," *Lab on a Chip*, vol. 16, no. 12, pp. 2168–2187, 2016.

[8] A. Bren and M. Eisenbach, "How signals are heard during bacterial chemotaxis: protein-protein interactions in sensory signal propagation," *Journal of Bacteriology*, vol. 182, no. 24, pp. 6865–6873, 2000.

[9] T. Kaya and H. Koser, "Direct upstream motility in *Escherichia coli*," *Biophysical Journal*, vol. 102, no. 7, pp. 1514–1523, 2012.

[10] T. Ishikawa, T. Shioiri, K. Numayama-Tsuruta, H. Ueno, Y. Imai, and T. Yamaguchi, "Separation of motile bacteria using drift velocity in a microchannel," *Lab on a Chip*, vol. 14, no. 5, pp. 1023–1032, 2014.

[11] J. A. Aufrecht, J. D. Fowlkes, A. N. Bible, J. Morrell-Falvey, M. J. Doktycz, and S. T. Retterer, "Pore-scale hydrodynamics influence the spatial evolution of bacterial biofilms in a microfluidic porous network," *PLoS One*, vol. 14, no. 6, Article ID e0218316, 2018.

[12] J. P. Gurung, M. Gel, and M. A. B. Baker, "Microfluidic techniques for separation of bacterial cells via taxis," *Microbial Cell*, vol. 7, no. 3, pp. 66–79, 2020.

[13] M. A. Bees, "Advances in bioconvection," *Annual Review of Fluid Mechanics*, vol. 52, pp. 449–476, 2020.

[14] V. A. Vladimirov, P. V. Denissenko, T. J. Pedley, M. Wu, and I. S. Moskalev, "Algal motility measured by a laser-based tracking method," *Marine and Freshwater Research*, vol. 51, pp. 589–600, 2000.

[15] V. A. Vladimirov, M. S. C. Wu, T. J. Pedley, P. V. Denissenko, and S. G. Zakhidova, "Measurement of cell velocity distributions in populations of motile algae," *Journal of Experimental Biology*, vol. 207, pp. 1203–1216, 2004.

[16] N. A. Hill and T. J. Pedley, "Bioconvection," *Fluid Dynamics Research*, vol. 37, pp. 1–20, 2005.

[17] T. Muhammad, H. Waqas, U. Farooq, and M. S. Alqarni, "Numerical simulation for melting heat transport in nanofluids due to quadratic stretching plate with nonlinear thermal radiation," *Case Studies in Thermal Engineering*, vol. 27, Article ID 101300, 2021.

[18] T. Muhammad, H. Waqas, U. Manzoor, U. Farooq, and Z. Fatima Rizvi, "On doubly stratified bioconvective transport of Jeffrey nanofluid with gyrotactic motile microorganisms," *Alexandria Engineering Journal*, vol. 61, 2021.

[19] T. Muhammad, S. Z. Alamri, H. Waqas, D. Habib, and R. Ellahi, "Bioconvection flow of magnetized carreau nanofluid under the influence of slip over a wedge with motile microorganisms," *Journal of Thermal Analysis and Calorimetry*, vol. 143, pp. 945–957, 2021.

[20] T. Muhammad, H. Waqas, S. A. Khan, R. Ellahi, and S. M. Sait, "Significance of nonlinear thermal radiation in 3D Eyring–powell nanofluid flow with Arrhenius activation energy," *Journal of Thermal Analysis and Calorimetry*, vol. 143, pp. 929–944, 2021.

[21] K. Naganthran, M. F. Md Basir, T. Thumma, E. O. Ige, R. Nazar, and I. Tlili, "Scaling group analysis of bioconvective micropolar fluid flow and heat transfer in a porous medium," *Journal of Thermal Analysis and Calorimetry*, vol. 143, no. 3, pp. 1943–1955, 2021.

[22] O. A. Bég, M. J. Uddin, T. A. Bég, A. Kadir, M. Shamshuddin, and M. Babaie, "Numerical study of self-similar natural convection mass transfer from a rotating cone in anisotropic porous media with Stefan blowing and Navier slip," *Indian Journal of Physics*, vol. 94, pp. 863–877, 2020.

[23] O. A. Bég, M. N. Kabir, M. J. Uddin, A. Izani Md Ismail, and Y. M. Alginahi, "Numerical investigation of Von Karman swirling bioconvective nanofluid transport from a rotating disk in a porous medium with Stefan blowing and anisotropic slip effects," *Proceedings—Institution of Mechanical Engineers Part C Journal of Mechanical Engineering Science*, vol. 234, no. 3-4, 2020.

[24] F. Tuz Zohra, M. J. Uddin, M. F. Basir, and A. I. M. Ismail, "Magnetohydrodynamic bio-nano-convective slip flow with Stefan blowing effects over a rotating disc," *Proceedings—Institution of Mechanical Engineers Part N Journal of Nanomaterials Nanoengineering and Nanosystems*, vol. 234, no. 3-4, pp. 83–97, 2020.

[25] F. T. Zohra, M. J. Uddin, and A. I. M. Ismail, "Magnetohydrodynamic bio-nanoconvective Naiver slip flow of micropolar fluid in a stretchable horizontal channel," *Heat Transfer—Asian Research*, vol. 48, no. 8, pp. 3636–3656, 2019.

[26] N. A. Amirsom, M. J. Uddin, M. D. Faisal Md Basir, A. I. M. Ismail, O. Anwar Bég, and A. Kadir, "Three-dimensional bioconvection nanofluid flow from a bi-axial stretching sheet with anisotropic slip," *Sains Malaysiana*, vol. 48, no. 5, pp. 1137–1149, 2019.

[27] N. Waisbord, C. T. Lefèvre, L. Bocquet, C. Ybert, and C. Cottin-Bizonne, "Destabilization of a flow focused suspension of magnetotactic bacteria," *Physical Review Fluids*, vol. 1, no. 5, Article ID 053203, 2016.

[28] N. S. Akbar and Z. H. Khan, "Magnetic field analysis in a suspension of gyrotactic microorganisms and nanoparticles over a stretching surface," *Journal of Magnetism and Magnetic Materials*, vol. 410, pp. 72–80, 2016.

[29] T. Chakraborty, K. Das, and P. K. Kundu, "Framing the impact of external magnetic field on bioconvection of a nanofluid flow containing gyrotactic microorganisms with convective boundary conditions," *Alexandria Engineering Journal*, vol. 57, no. 1, pp. 61–71, 2018.

[30] D. Pal and S. K. Mondal, "Influence of chemical reaction and nonlinear thermal radiation on bioconvection of nanofluid containing gyrotactic microorganisms with magnetic field," *Bionanoscience*, vol. 8, pp. 1065–1080, 2018.

[31] W. N. Mutuku and O. D. Makinde, "Hydromagnetic bioconvection of nanofluid over a permeable vertical plate due to gyrotactic microorganisms," *Computers & Fluids*, vol. 95, pp. 88–97, 2014.

[32] N. Biswas, A. Datta, N. K. Manna, D. K. Mandal, and R. S. R. Gorla, "Thermo-bioconvection of oxytactic microorganisms in porous media in the presence of magnetic field," *International Journal of Numerical Methods for Heat and Fluid Flow*, vol. 31, 2020.

[33] S. A. Shehzad, T. Mushtaq, Z. Abbas, A. Rauf, S. U. Khan, and I. Tlili, "Dynamics of bioconvection flow of micropolar nanoparticles with Cattaneo-Christov expressions," *Applied Mathematics and Mechanics*, vol. 41, pp. 1333–1344, 2020.

[34] S. Xun, J. Zhao, L. Zheng, and X. Zhang, "Bioconvection in rotating system immersed in nanofluid with temperature dependent viscosity and thermal conductivity," *International Journal of Heat and Mass Transfer*, vol. 111, pp. 1001–1006, 2017.

[35] H. Waqas, M. Imran, T. Muhammad, S. M. Sait, and R. Ellahi, "Numerical investigation on bioconvection flow of Oldroyd-B nanofluid with nonlinear thermal radiation and motile microorganisms over rotating disk," *Journal of Thermal Analysis and Calorimetry*, vol. 145, 2020.

[36] S. Saleem, H. Rafiq, A. Al-Qahtani, M. A. El-Aziz, M. Y. Malik, and I. L. Animasaun, "Magneto Jeffrey nanofluid bioconvection over a rotating vertical cone due to gyrotactic microorganism," *Mathematical Problems in Engineering*, vol. 2019, Article ID 3478037, 11 pages, 2019.

[37] N. S. Khan, Q. Shah, A. Bhaumik, P. Kumam, P. Thounthong, and I. Amiri, "Entropy generation in bioconvection nanofluid flow between two stretchable rotating disks," *Scientific Reports*, vol. 10, p. 4448, 2020.

[38] E. M. Sparrow and R. D. Cess, "Magnetohydrodynamic flow and heat transfer about a rotating disk," *Journal of Applied Mechanics, Transactions ASME*, vol. 29, no. 1, pp. 181–187, 1960.

[39] N. A. Latiff, M. J. Uddin, and A. I. Md Ismail, "Stefan blowing effect on bioconvective flow of nanofluid over a solid rotating stretchable disk," *Propulsion and Power Research*, vol. 5, 2016.

[40] N. Tarakaramu and P. V. Satya Narayana, "Chemical reaction effects on bio-convection nanofluid flow between two parallel plates in rotating system with variable viscosity: a numerical study," *Journal of Applied and Computational Mechanics*, vol. 5, no. 4, pp. 791–803, 2019.

[41] S. Parvanian, S. M. Mostafavi, and M. Aghashiri, "Multifunctional nanoparticle developments in cancer diagnosis and treatment," *Sensing and Bio-Sensing Research*, vol. 13, pp. 81–87, 2017.

[42] K. O. Saunders, E. Lee, R. Parks et al., "Neutralizing antibody vaccine for pandemic and pre-emergent coronaviruses," *Nature*, vol. 594, pp. 553–559, 2021.

[43] Y. He, X. Zhang, and H. Yu, "Gold nanoparticles-based colorimetric and visual creatinine assay," *Microchimica Acta*, vol. 182, no. 11, pp. 2037–2043, 2015.

[44] E. O. Ige, R. K. Arun, P. Singh, M. Gope, R. Saha, N. Chanda et al., "Water desalination using graphene oxide-embedded paper microfluidics," *Microfluidics Nanofluidics*, vol. 23, no. 6, pp. 1–8, 2019.

[45] M. An, M. Li, J. Xi, and H. Liu, "Silica nanoparticle as a lymph node targeting platform for vaccine delivery," *ACS Applied Materials & Interfaces*, vol. 28, no. 9, pp. 23466–23475, 2017.

[46] S. Dhital and N. R. Vyavahare, "Nanoparticle-based targeted delivery of pentagalloyl glucose reverses elastase-induced abdominal aortic aneurysm and restores aorta to the healthy state in mice," *PLoS One*, vol. 15, no. 3, Article ID e0227165, 2020.

[47] G. B. Lim, "Nanotherapy for abdominal aortic aneurysm," *Nature Reviews Cardiology*, vol. 16, p. 71, 2019.

[48] R. Vinhas, R. Mendes, A. R. Fernandes, and P. V. Baptista, "Nanoparticles-emerging potential for managing leukemia and lymphoma," *Frontiers in Bioengineering and Biotechnology*, vol. 5, no. 1–10, p. 79, 2017.

[49] M. Lundqvist, C. Augustsson, M. Lilja et al., "The nanoparticle protein corona formed in human blood or human blood fractions," *PLoS One*, vol. 12, no. 4, Article ID e0175871, 2017.

[50] J. Gomez-Marquez and K. Hamad-Schifferli, "Local development of nanotechnology-based diagnostics," *Nature Nanotechnology*, vol. 16, pp. 484–486, 2021.

[51] O. A. Bég, M. J. Uddin, M. M. Rashidi, and N. Kavyani, "Double-diffusive radiative magnetic mixed convective slip flow with Biot and Richardson number effects," *Journal of Engineering and Thermophysics*, vol. 23, no. 2, pp. 79–97, 2014.

[52] M. J. Uddin, O. A. Bég, and A. I. Ismail, "Radiative convective nanofluid flow past a stretching/shrinking sheet with slip effects," *Journal of Thermophysics and Heat Transfer*, vol. 29, no. 3, pp. 513–523, 2015.

[53] M. J. Uddin, M. N. Kabir, Y. Alginahi, and O. A. Bég, "Numerical solution of bio-nano-convection transport from a horizontal plate with blowing and multiple slip effects," *Proceedings of the Institution of Mechanical Engineers Part C Journal of Mechanical Engineering Science*, vol. 233, no. 19-20, pp. 6910–6927, 2019.

[54] M. J. Uddin, N. A. Amirsom, O. A. Bég, and A. I. Ismail, "Computation of bio-nano-convection power law slip flow from a needle with blowing effects in a porous medium," *Waves in Random and Complex Media*, vol. 32, 2022.

[55] J. Bodduna, M. P. Mallesh, C. S. Balla, and S. A. Shehzad, "Activation energy process in bioconvection nanofluid flow through porous cavity," *Journal of Porous Media*, vol. 25, no. 4, pp. 37–51, 2022.

[56] R. Alluguvelli, C. S. Balla, K. Naikoti, and O. D. Makinde, "Nanofluid bioconvection in porous enclosure with viscous dissipation," *Indian Journal of Pure and Applied Physics*, vol. 60, no. 1, pp. 78–89, 2022.

[57] C. S. Balla, R. Alluguvelli, K. Naikoti, and O. D. Makinde, "Effect of chemical reaction on bioconvective flow in oxytactic microorganisms suspended porous cavity," *Journal of Applied and Computational Mechanics*, vol. 6, no. 3, pp. 653–664, 2020.

[58] C. Haritha, B. C. Shekar, and N. Kishan, "MHD natural convection heat transfer in a porous square cavity filled by nanofluids with viscous dissipation," *Journal of Nanofluids*, vol. 7, no. 5, pp. 928–938, 2018.

[59] C. Balla and K. Naikoti, "Numerical solution of MHD bioconvection in a porous square cavity due to oxytactic microorganisms," *Applications and Applied Mathematics: An International Journal (AAM)*, vol. 14, no. 4, 2019.

[60] B. Jamuna and C. S. Balla, "Bioconvection in a porous square cavity containing gyrotactic microorganisms under the effects of heat generation/absorption," *Proceedings of the Institution of Mechanical Engineers Part E Journal of Process Mechanical Engineering*, vol. 235, no. 5, pp. 1534–1544, 2021.

[61] C. Wang, H. Lin, and C. Ye, "Functional magnetic nanoparticles for facile viable but nonculturable bacteria separation and purification," *Frontiers of Environmental Science & Engineering*, vol. 10, no. 6, pp. 1–6, 2016.

[62] O. Anwar Beg, B. Vasu, T. Sochi, and V. R. Prasad, "Keller Box and smoothed particle hydrodynamic numerical simulation of two-phase transport in blood purification auto-transfusion dialysis hybrid device with Stokes and Darcy number effects," *Journal of Advanced Biotechnology and Bioengineering*, vol. 1, pp. 80–100, 2013.

[63] T. Sajid, M. Sagheer, S. Hussain, and F. Shahzad, "Impact of double-diffusive convection and motile gyrotactic microorganisms on magnetohydrodynamics bioconvection tangent hyperbolic nanofluid," *Open Physics*, vol. 18, pp. 74–88, 2020.

[64] Z. Abdelmalek, I. Khan, M. Waleed Ahmed Khan, K. Ur Rehman, and E. S. M. Sherif, "Computational analysis of nano-fluid due to a non-linear variable thicked stretching sheet subjected to Joule heating and thermal radiation," *Journal of Materials Research and Technology*, vol. 9, no. 5, pp. 11035–11044, 2020.

[65] M. J. Uddin, Y. Alginahi, O. A. Bég, and M. N. Kabir, "Numerical solutions for gyrotactic bioconvection in nanofluid-saturated porous media with Stefan blowing and multiple slip effects," *Computers & Mathematics with Applications*, vol. 72, no. 10, pp. 2562–2581, 2016.

[66] S. S. Motsa, P. Sibanda, and S. Shateyi, "A new spectral-homotopy analysis method for solving a nonlinear second order BVP," *Communications in Nonlinear Science and Numerical Simulation*, vol. 15, no. 9, pp. 2293–2302, 2010.

[67] S. S. Motsa, S. Shateyi, G. T. Marewo, and P. Sibanda, "An improved spectral homotopy analysis method for MHD flow in a semi-porous channel," *Numerical Algorithms*, vol. 60, pp. 463–481, 2012.

[68] H. Saberi Nik, S. Effati, S. S. Motsa, and M. Shirazian, "Spectral homotopy analysis method and its convergence for solving a class of nonlinear optimal control problems," *Numerical Algorithms*, vol. 65, pp. 171–194, 2014.

[69] P. E. Gill, L. O. Jay, M. W. Leonard, L. R. Petzold, and V. Sharma, "An SQP method for the optimal control of large-scale dynamical systems," *Journal of Computational and Applied Mathematics*, vol. 120, pp. 197–213, 2000.

[70] Z. Pashazadeh Atabakan, A. Klçman, and A. Kazemi Nasab, "On spectral homotopy analysis method for solving linear Volterra and Fredholm integro differential equations," *Abstract and Applied Analysis*, vol. 2012, Article ID 960289, 16 pages, 2012.

[71] Z. Pashazadeh Atabakan, A. Kazemi Nasab, A. Kiliçman, and Z. K. Eshkuvatov, "Numerical solution of nonlinear Fredholm integro-differential equations using spectral homotopy analysis method," *Mathematical Problems in Engineering*, vol. 2013, Article ID 674364, 9 pages, 2013.

[72] E. O. Ige, F. H. Oyelami, E. S. Adedipe et al., "Analytical simulation of nanoparticle-embedded blood flow control with magnetic field influence through spectra homotopy analysis method," *International Journal of Modern Physics B*, vol. 35, no. 22, 2021.

[73] P. G. Dlamini, M. Khumalo, and S. S. Motsa, "A note on the multi-stage spectral relaxation method for chaos control and synchronization," *International Journal of Nonlinear Sciences and Numerical Stimulation*, vol. 15, no. 5, pp. 289–298, 2014.

[74] M. B. K. Moorthy and K. Senthilvadivu, "Soret and Dufour effects on natural convection flow past a vertical surface in a porous medium with variable viscosity," *Journal of Applied Mathematics*, vol. 2012, Article ID 634806, 15 pages, 2012.